nature

https://doi.org/10.1038/s41586-021-03738-2

Accelerated Article Preview

# SARS-CoV-2 mRNA vaccines induce persistent human germinal centre responses

Received: 8 March 2021

Accepted: 18 June 2021

Accelerated Article Preview Published online 28 June 2021

Cite this article as: Turner, J. S. et al. SARS-CoV-2 mRNA vaccines induce persistent human germinal centre responses. *Nature* https://doi.org/10.1038/s41586-021-03738-2 (2021).

**Jackson S. Turner, Jane A. O'Halloran, Elizaveta Kalaidina, Wooseob Kim, Aaron J. Schmitz, Julian Q. Zhou, Tingting Lei, Mahima Thapa, Rita E. Chen, James Brett Case, Fatima Amanat, Adriana M. Rauseo, Alem Haile, Xuping Xie, Michael K. Klebert, Teresa Suessen, William D. Middleton, Pei-Yong Shi, Florian Krammer, Sharlene A. Teefey, Michael S. Diamond, Rachel M. Presti & Ali H. Ellebedy**

Article

# SARS-CoV-2 mRNA vaccines induce persistent human germinal centre responses

https://doi.org/10.1038/s41586-021-03738-2

Received: 8 March 2021

Accepted: 18 June 2021

Published online: 28 June 2021

Jackson S. Turner[1,12], Jane A. O'Halloran[2,12], Elizaveta Kalaidina[3], Wooseob Kim[1], Aaron J. Schmitz[1], Julian Q. Zhou[1], Tingting Lei[1], Mahima Thapa[1], Rita E. Chen[1,4], James Brett Case[4], Fatima Amanat[5,6], Adriana M. Rauseo[2], Alem Haile[7], Xuping Xie[8], Michael K. Klebert[7], Teresa Suessen[9], William D. Middleton[9], Pei-Yong Shi[8], Florian Krammer[5], Sharlene A. Teefey[9], Michael S. Diamond[4,10,11], Rachel M. Presti[2,10]✉ & Ali H. Ellebedy[1,10,11]✉

Severe Acute Respiratory Syndrome Coronavirus 2 (SARS-CoV-2) messenger RNA (mRNA)-based vaccines are ~95% effective in preventing coronavirus disease 2019[1–5]. The dynamics of antibody secreting plasmablasts (PBs) and germinal centre (GC) B cells induced by these vaccines in humans remain unclear. We examined antigen-specific B cell responses in peripheral blood (n=41) and draining lymph nodes (LNs) in 14 individuals who received two doses of BNT162b2, an mRNA-based vaccine encoding full-length SARS-CoV-2 spike (S) gene[1]. Circulating IgG- and IgA-secreting PBs targeting the S protein peaked one week after the second immunization then declined, becoming undetectable three weeks later. These PB responses preceded maximal levels of serum anti-S binding and neutralizing antibodies to an early circulating SARS-CoV-2 strain as well as emerging variants, especially in individuals previously infected with SARS-CoV-2, who produced the most robust serologic responses. By examining fine needle aspirates (FNAs) of draining axillary LNs, we identified GC B cells that bound S protein in all participants sampled after primary immunization. Remarkably, high frequencies of S-binding GC B cells and PBs were sustained in these draining LNs for at least twelve weeks after the booster immunization. S-binding GC B cell-derived monoclonal antibodies predominantly targeted the receptor binding domain of the S protein, with fewer clones binding to the N-terminal domain or to epitopes shared with the S proteins of the human betacoronaviruses OC43 and HKU1. The latter cross-reactive B cell clones had higher levels of somatic hypermutation compared to those that only recognized SARS-CoV-2 S protein, suggesting a memory B cell origin. Our studies demonstrate that SARS-CoV-2 mRNA-based vaccination of humans induces a persistent GC B cell response, enabling the generation of robust humoral immunity.

The concept of using mRNAs as vaccines was introduced over 30 years ago[6,7]. Key refinements that improved the biological stability and translation capacity of exogenous mRNA enabled development of these molecules as vaccines[8,9]. The emergence of SARS-CoV-2 in December, 2019 and the ensuing pandemic has unveiled the potential of this platform[9–11]. Hundreds of millions of people have received one of the two SARS-CoV-2 mRNA-based vaccines that were granted emergency use authorization by the FDA in December, 2020. Both vaccines demonstrated remarkable immunogenicity in phase 1/2 studies and efficacy in phase 3 studies[1–4,12–14]. Whether these vaccines induce robust and persistent germinal center (GC) reactions that are critical for generating high-affinity and durable antibody responses has not been examined in humans. To address this question, we conducted an observational study of 41 healthy adults (8 with history of confirmed SARS-CoV-2 infection) who received the Pfizer-BioNTech SARS-CoV-2 mRNA vaccine (BNT162b2) (Extended Data Tables 1, 2). Blood samples were collected at baseline and at weeks 3 (pre-boost), 4, 5, 7, and 15 after the first immunization (Fig. 1a). FNAs of the draining axillary LNs were collected from 14 participants (none with history of SARS-CoV-2 infection) at weeks 3 (pre-boost), 4, 5, 7, and 15 after the first immunization (Fig. 1a).

[1]Department of Pathology and Immunology, Washington University School of Medicine, St Louis, MO, USA. [2]Division of Infectious Diseases, Department of Internal Medicine, Washington University School of Medicine, St Louis, MO, USA. [3]Division of Allergy and Immunology, Department of Internal Medicine, Washington University School of Medicine, St Louis, MO, USA. [4]Department of Medicine, Washington University School of Medicine, St Louis, MO, USA. [5]Department of Microbiology, Icahn School of Medicine at Mount Sinai, New York, NY, USA. [6]Graduate School of Biomedical Sciences, Icahn School of Medicine at Mount Sinai, New York, NY, USA. [7]Clinical Trials Unit, Washington University School of Medicine, St Louis, MO, USA. [8]University of Texas Medical Branch, Galveston, TX, USA. [9]Mallinckrodt Institute of Radiology, Washington University School of Medicine, St Louis, MO, USA. [10]Center for Vaccines and Immunity to Microbial Pathogens, Washington University School of Medicine, St Louis, MO, USA. [11]The Andrew M. and Jane M. Bursky Center for Human Immunology & Immunotherapy Programs, St Louis, USA. [12]These authors contributed equally: Jackson S. Turner, Jane A. O'Halloran. ✉e-mail: prestir@wustl.edu; ellebedy@wustl.edu

Antibody-secreting PBs in blood that bound SARS-CoV-2 S protein were measured by enzyme-linked immune absorbent spot (ELISpot) assay. SARS-CoV-2-S-specfic IgG- and IgA-secreting PBs were detected three weeks after primary immunization in 24 of 33 participants with no history of SARS-CoV-2 infection but 0 of 8 participants previously infected with SARS-CoV-2. PBs peaked in blood during the first week after boosting (week 4 after primary immunization), with frequencies varying widely from 3 to 4,100 S-binding PBs per $10^6$ PBMC (Fig. 1b, c). Plasma IgG antibody titers against S measured by ELISA increased in all participants over time, reaching peak geometric mean half-maximal binding titers (GMBTs) of 5,567 and 15,850 5 weeks after immunization among participants without and with history of SARS-CoV-2 infection, respectively, with a subsequent decline by 15 weeks after immunization. Anti-S IgA titers and IgG titers against the receptor binding domain (RBD) of S showed similar kinetics, reaching peak GMBTs of 172 and 739 for anti-S IgA and 4,501 and 7,965 for anti-RBD IgG among participants without and with history of SARS-CoV-2 infection, respectively before declining. IgM responses were weaker and more transient, peaking 4 weeks after immunization among participants without history of SARS-CoV-2 infection with a GMBT of 78 and were undetectable in all but two previously infected participants (Fig. 1d, Extended Data Fig. 1a).

The functional quality of serum antibody was measured using high-throughput focus reduction neutralization tests[15] on Vero-TMPRSS2 cells against three authentic infectious SARS-CoV-2 strains with sequence variations in the S gene[16,17]: (a) a Washington strain (2019n-CoV/USA) with a prevailing D614G substitution (WA1/2020 D614G); (b) a B.1.1.7 isolate with signature changes in the spike gene[18], including the 69–70 and 144–145 deletions and N501Y, A570D, D614G and P681H substitutions; and (c) a chimeric SARS-CoV-2 with a B.1.351 spike gene in the Washington strain background (Wash B.1.351) that contained the following changes: D80A, 242-244 deletion, R246I, K417N, E484K, N501Y, D614G and A701V. Serum neutralizing titers increased markedly in participants without history of SARS-CoV-2 infection following boosting, with geometric mean neutralization titers (GMNTs) against WA1/2020 D614G of 58 three weeks after primary immunization and 572 two or four weeks after boost (five or seven weeks after primary immunization). Neutralizing titers against B.1.1.7 and B.1.351 variants were lower, with GMNTs of 49 and 373 against B.1.1.7 and 36 and 137 against B.1.351 after primary and secondary immunization, respectively. In participants with a history of prior SARS-CoV-2 infection, neutralizing titers against all three viruses were detected at baseline (GMNTs of 241.8, 201.8, and 136.7 against WA1/2020 D614G, B.1.1.7, and B.1.351 respectively). In these participants, neutralizing titers increased more rapidly and to higher levels after immunization, with GMNTs of 4,544, 3,584, and 1,897 against WA1/2020 D614G, B.1.1.7, and B.1.351, respectively after primary immunization, and 9,381, 9,351, and 2,749 against WA1/2020 D614G, B.1.1.7, and B.1.351 respectively after secondary immunization. These GMNTs were 78-, 73-, and 53-fold higher after primary immunization and 16-, 25-, and 20-fold higher after boosting against WA1/2020 D614G, B.1.1.7, and B.1.351, respectively than participants without history of SARS-CoV-2 infection. (Extended Data Fig. 1b).

The BNT162b2 vaccine is injected into the deltoid muscle, which drains primarily to the lateral axillary LNs. Ultrasonography was used to identify and guide FNA of accessible axillary nodes on the side of immunization approximately 3 weeks after primary immunization. In 5 of the 14 participants, a second draining LN was identified and sampled following secondary immunization (Fig. 2a). GC B cells, defined as $CD19^+$ $CD3^-$ $IgD^{lo}$ $Bcl6^+$ $CD38^{int}$ lymphocytes, were detected in all LNs (Fig. 2b, d, Extended Data Fig. 2a, Extended Data Table 3). FNA samples were co-stained with two fluorescently labeled S probes to detect S-binding GC B cells. A control tonsillectomy sample with a high frequency of GC B cells collected prior to the SARS-CoV-2 pandemic from an unrelated donor was stained as a negative control. S-binding GC B cells were detected in FNAs from all 14 participants following primary immunization. The kinetics of the GC response varied among participants, but S-binding GC B cell frequencies increased at least transiently in all participants after boosting and persisted at high frequency in most individuals for at least 7 weeks. Notably, S-binding GC B cells remained at or near their peak frequency 15 weeks after immunization in 8 of the 10 participants sampled at that time point, and these prolonged GC responses had high proportions of S-binding cells (Fig. 2c–e, Extended Data Fig. 2b).

To evaluate the domains targeted by the S protein-specific GC response after vaccination, we generated recombinant monoclonal antibodies (mAbs) from single-cell sorted S-binding GC B cells (defined by the surface marker phenotype $CD19^+$ $CD3^-$ $IgD^{lo}$ $CD20^{hi}$ $CD38^{int}$ $CD71^+$ $CXCR5^+$ lymphocytes) from three of the participants one week after boosting (Extended Data Fig. 2a). Fifteen, five, and seventeen S-binding, clonally distinct mAbs were generated from participants 07, 20 (LN1), and 22, respectively (Extended Data Table 4). Of the 37 S-binding mAbs, 17 bound RBD, 6 recognized the N-terminal domain, and 3 were cross-reactive with spike proteins from seasonal betacoronavirus OC43; 2 of these mAbs also bound spike from seasonal betacoronavirus HKU1 (Fig. 3a). Clonal relatives of 14 of 15, 1 of 5, and 12 of 17 of the S-binding mAbs were identified among bulk-sorted total PBs from PBMCs and GC B cells 4 weeks after immunization from participants 07, 20, and 22, respectively (Fig. 3b, Extended Data Figs. 2c, 3a, b, and Extended Data Tables 5, 6). Clones related to S-binding mAbs had significantly increased mutation frequencies in their immunoglobulin heavy chain variable region (*IGHV*) genes compared to previously published naïve B cells, particularly those related to mAbs that cross-reacted with seasonal betacoronaviruses (Fig. 3c, d).

In addition to GC B cells, robust PB responses were detected in the draining LNs of all 14 participants in the FNA cohort. S-binding PBs, defined as $CD19^+$ $CD3^-$ $IgD^{lo}$ $CD20^{lo}$ $CD38^+$ $CD71^+$ $Blimp1^+$ lymphocytes, were detected in all LNs sampled and increased in frequency after boosting (Extended Data Fig. 4a, b). The detected PBs were unlikely a contaminant of blood because $CD14^+$ monocyte/granulocyte frequencies were below 1% in all FNA samples, well below the 10% threshold we previously established[19] (Extended Data Table 3). Moreover, S-binding PBs were detected in FNA samples 5, 7, and 15 weeks after immunization, when they had become undetectable in blood from all participants in the cohort. The vast majority of S-binding LN PBs were isotype-switched 4 weeks after primary immunization, and IgA-switched cells accounted for 25% or more of the PBs in 6 of 14 participants (Extended Data Fig. 4c, d).

This study evaluated whether SARS-CoV-2 mRNA-based vaccines induce antigen-specific PB and GC B cell responses in humans. The vaccine induced a strong IgG-dominated PB response in blood that peaked one week after the booster immunization. In the draining LNs, we detected robust SARS-CoV-2 S-binding GC B cell and PB responses in aspirates from all 14 participants. These responses were detectable after the first immunization but greatly expanded after the booster injection. Notably, S-binding GC B cells and PBs persisted for at least 15 weeks after the first immunization (12 weeks after secondary immunization) in 8 of the 10 participants sampled at that time point. These responses to mRNA vaccination are superior to those seen after seasonal influenza virus vaccination in humans[19], where hemagglutinin-binding GC B cells were detected in only three of eight participants. More robust GC responses are consistent with antigen dissemination to multiple LNs and the self-adjuvating characteristics of the mRNA/lipid nanoparticle vaccine platform compared to nonadjuvanted inactivated vaccines used for seasonal influenza virus vaccination[7,20,21]. Our data in humans corroborate reports demonstrating the induction of potent GC responses by SARS-CoV-2 mRNA-based vaccines in mice[22,23].

This is the first study to provide direct evidence for the induction of a persistent antigen specific GC B cell response after vaccination in

humans. Dynamics of GC B cell responses vary widely depending on the model system in which they are studied, although the most active period of the response usually occurs over the course of a few weeks. Primary alum-adjuvanted protein immunization of mice typically leads to GC responses that peak 1–2 weeks after immunization and contract at least 10-fold within 5–7 weeks[24–26]. GC responses induced by immunization with more robust adjuvants such as sheep red blood cells, complete Freund's adjuvant, or saponin-based adjuvants tend to peak slightly later, 2–4 weeks after vaccination, and can persist at low frequencies for several months[27–33]. Although studies of extended durability are rare, antigen-specific GC B cells have been found to persist for at least one year, albeit at very low levels[28,30]. In this study, we show SARS-CoV-2 mRNA vaccine-induced GC B cells are maintained at or near peak frequencies for at least 12 weeks after secondary immunization.

The persistence of S-binding GC B cells and PBs in draining LNs is a positive indicator for induction of long-lived plasma cell responses[25]. Future studies will be needed to examine whether mRNA vaccination induces a robust S-specific long-lived plasma cell compartment in the bone marrow. As part of such studies, it will be critical to generate a comprehensive set of mAbs derived from PBs and GC B cells isolated from multiple time points to define the breadth of the B cell response elicited by this vaccine. None of the 14 participants in our study who underwent FNA of draining LNs had a history of SARS-CoV-2 infection. Thus, further comparison of vaccine-induced GC responses from naïve and previously infected individuals will be informative. Finally, the work presented here focuses on the B cell component of the GC reaction. A robust T follicular helper response sustains the GC reaction[34,35]. As such, studies are planned to interrogate the magnitude, specificity, and durability of the T follicular helper cell response after SARS-CoV-2 mRNA vaccination in humans.

A preliminary observation from our study is the dominance of RBD-targeting clones among responding GC B cells. In a more detailed analysis of these RBD-binding mAbs, we assessed their *in vitro* inhibitory capacity against the WA1/2020 D614G strain using an authentic SARS-CoV-2 neutralization assay; five showed high neutralization potency with 80% neutralization values of less than 100 ng/mL[36]. For the most part, RBD-binding clones harbored few (<3) non-synonymous nucleotide substitutions in the immunoglobulin heavy chain variable genes, indicating that they originated from recently engaged naïve B cells. This contrasts with the three cross-reactive GC B cell clones that recognized conserved epitopes within the spike proteins of betacoronaviruses. These cross-reactive clones had significantly higher mutation frequencies, suggesting a memory B cell origin. These data are consistent with previous findings from seasonal influenza virus vaccination in humans showing that the GC reaction can engage pre-existing memory B cells directed against conserved epitopes as well as naïve clones targeting novel epitopes[19]. However, these cross-reactive clones were not identified in all individuals and comprised a small fraction of responding B cells, consistent with a similar analysis of SARS-CoV-2 mRNA vaccine-induced plasmablasts[37]. Overall, our data demonstrate a remarkable capacity of SARS-CoV-2 mRNA-based vaccines to induce robust and prolonged GC reactions. The induced GC reaction recruited cross-reactive memory B cells as well as newly engaged clones that target unique epitopes within SARS-CoV-2 S protein. Elicitation of high affinity and durable protective antibody responses is a hallmark of a successful humoral immune response to vaccination. By inducing robust GC reactions, SARS-CoV-2 mRNA-based vaccines are on track for achieving this outcome.

## Online content

Any methods, additional references, Nature Research reporting summaries, source data, extended data, supplementary information, acknowledgements, peer review information; details of author contributions and competing interests; and statements of data and code availability are available at https://doi.org/10.1038/s41586-021-03738-2.


1. Mulligan, M. J. *et al*. Phase I/II study of COVID-19 RNA vaccine BNT162b1 in adults. *Nature* **586**, 589–593 (2020).
2. Jackson, L. A. *et al*. An mRNA Vaccine against SARS-CoV-2 — Preliminary Report. *N. Engl. J. Med*. **383**, 1920–1931 (2020).
3. Sahin, U. *et al*. COVID-19 vaccine BNT162b1 elicits human antibody and TH1 T cell responses. *Nature* **586**, 594–599 (2020).
4. Polack, F. P. *et al*. Safety and Efficacy of the BNT162b2 mRNA Covid-19 Vaccine. *N. Engl. J. Med*. **383**, 2603–2615 (2020).
5. Baden, L. R. *et al*. Efficacy and Safety of the mRNA-1273 SARS-CoV-2 Vaccine. *N. Engl. J. Med*. **384**, 403–416 (2021).
6. Zhou, X. *et al*. Self-replicating Semliki Forest virus RNA as recombinant vaccine. *Vaccine* **12**, 1510–1514 (1994).
7. Cagigi, A. & Loré, K. Immune Responses Induced by mRNA Vaccination in Mice, Monkeys and Humans. *Vaccines* **9**, 61 (2021).
8. Karikó, K. *et al*. Incorporation of Pseudouridine Into mRNA Yields Superior Nonimmunogenic Vector With Increased Translational Capacity and Biological Stability. *Mol. Ther*. **16**, 1833–1840 (2008).
9. Schlake, T., Thess, A., Fotin-Mleczek, M. & Kallen, K.-J. Developing mRNA-vaccine technologies. *RNA Biol*. **9**, 1319–1330 (2012).
10. Graham, B. S., Mascola, J. R. & Fauci, A. S. Novel Vaccine Technologies: Essential Components of an Adequate Response to Emerging Viral Diseases. *JAMA* **319**, 1431 (2018).
11. Bettini, E. & Locci, M. SARS-CoV-2 mRNA Vaccines: Immunological Mechanism and Beyond. *Vaccines* **9**, 147 (2021).
12. Amit, S., Regev-Yochay, G., Afek, A., Kreiss, Y. & Leshem, E. Early rate reductions of SARS-CoV-2 infection and COVID-19 in BNT162b2 vaccine recipients. *The Lancet* **397**, 875–877 (2021).
13. Dagan, N. *et al*. BNT162b2 mRNA Covid-19 Vaccine in a Nationwide Mass Vaccination Setting. *N. Engl. J. Med*. NEJMoa2101765 (2021) https://doi.org/10.1056/NEJMoa2101765
14. Vasileiou, E. *et al*. Effectiveness of First Dose of COVID-19 Vaccines Against Hospital Admissions in Scotland: National Prospective Cohort Study of 5.4 Million People. *SSRN Electron. J.* (2021) https://doi.org/10.2139/ssrn.3789264
15. Case, J. B. *et al*. Neutralizing Antibody and Soluble ACE2 Inhibition of a Replication-Competent VSV-SARS-CoV-2 and a Clinical Isolate of SARS-CoV-2. *Cell Host Microbe* **28**, 475-485.e5 (2020).
16. Liu, Y. *et al*. Neutralizing Activity of BNT162b2-Elicited Serum — Preliminary Report. *N. Engl. J. Med*. NEJMc2102017 (2021) https://doi.org/10.1056/NEJMc2102017
17. Chen, R. E. *et al*. Resistance of SARS-CoV-2 variants to neutralization by monoclonal and serum-derived polyclonal antibodies. *Nat. Med*. (2021) https://doi.org/10.1038/s41591-021-01294-w
18. Leung, K., Shum, M. H., Leung, G. M., Lam, T. T. & Wu, J. T. Early transmissibility assessment of the N501Y mutant strains of SARS-CoV-2 in the United Kingdom, October to November 2020. *Eurosurveillance* **26**, (2021).
19. Turner, J. S. *et al*. Human germinal centres engage memory and naive B cells after influenza vaccination. *Nature* **586**, 127–132 (2020).
20. Pardi, N. *et al*. Expression kinetics of nucleoside-modified mRNA delivered in lipid nanoparticles to mice by various routes. *J. Controlled Release* **217**, 345–351 (2015).
21. Liang, F. *et al*. Efficient Targeting and Activation of Antigen-Presenting Cells In Vivo after Modified mRNA Vaccine Administration in Rhesus Macaques. *Mol. Ther*. **25**, 2635–2647 (2017).
22. Tai, W. *et al*. A novel receptor-binding domain (RBD)-based mRNA vaccine against SARS-CoV-2. *Cell Res*. **30**, 932–935 (2020).
23. Lederer, K. *et al*. SARS-CoV-2 mRNA Vaccines Foster Potent Antigen-Specific Germinal Center Responses Associated with Neutralizing Antibody Generation. *Immunity* **53**, 1281-1295.e5 (2020).
24. Kaji, T. *et al*. Distinct cellular pathways select germline-encoded and somatically mutated antibodies into immunological memory. *J. Exp. Med*. **209**, 2079–97 (2012).
25. Weisel, F. J., Zuccarino-Catania, G. V., Chikina, M. & Shlomchik, M. J. A Temporal Switch in the Germinal Center Determines Differential Output of Memory B and Plasma Cells. *Immunity* **44**, 116–130 (2016).
26. Good-Jacobson, K. L. *et al*. Regulation of germinal center responses and B-cell memory by the chromatin modifier MOZ. *Proc. Natl. Acad. Sci*. **111**, 9585–9590 (2014).
27. Bachmann, M. F., Odermatt, B., Hengartner, H. & Zinkernagel, R. M. Induction of long-lived germinal centers associated with persisting antigen after viral infection. *J. Exp. Med*. **183**, 2259–2269 (1996).
28. Dogan, I. *et al*. Multiple layers of B cell memory with different effector functions. *Nat. Immunol*. **10**, 1292–1299 (2009).
29. Rothaeusler, K. & Baumgarth, N. B-cell fate decisions following influenza virus infection. *Eur. J. Immunol*. **40**, 366–377 (2010).
30. Pape, K. A., Taylor, J. J., Maul, R. W., Gearhart, P. J. & Jenkins, M. K. Different B cell populations mediate early and late memory during an endogenous immune response. *Science* **331**, 1203–1207 (2011).
31. Turner, J. S., Benet, Z. L. & Grigorova, I. Transiently antigen primed B cells can generate multiple subsets of memory cells. *PLoS ONE* **12**, e0183877–e0183877 (2017).
32. Havenar-Daughton, C. *et al*. Rapid Germinal Center and Antibody Responses in Non-human Primates after a Single Nanoparticle Vaccine Immunization. *Cell Rep*. **29**, 1756-1766.e8 (2019).
33. Cirelli, K. M. *et al*. Slow Delivery Immunization Enhances HIV Neutralizing Antibody and Germinal Center Responses via Modulation of Immunodominance. *Cell* **177**, 1153-1171.e28 (2019).

34. Qi, H., Cannons, J. L., Klauschen, F., Schwartzberg, P. L. & Germain, R. N. SAP-controlled T-B cell interactions underlie germinal centre formation. *Nature* **455**, 764–9 (2008).
35. Johnston, R. J. *et al*. Bcl6 and Blimp-1 Are Reciprocal and Antagonistic Regulators of T Follicular Helper Cell Differentiation. *Science* **325**, 1006–1010 (2009).
36. Schmitz, A. J. *et al*. *A public vaccine-induced human antibody protects against SARS-CoV-2 and emerging variants*. http://biorxiv.org/lookup/doi/10.1101/2021.03.24.436864 (2021) https://doi.org/10.1101/2021.03.24.436864.
37. Amanat, F. *et al*. *The plasmablast response to SARS-CoV-2 mRNA vaccination is dominated by non-neutralizing antibodies that target both the NTD and the RBD*. http://medrxiv.org/lookup/doi/10.1101/2021.03.07.21253098 (2021) https://doi.org/10.1101/2021.03.07.21253098.

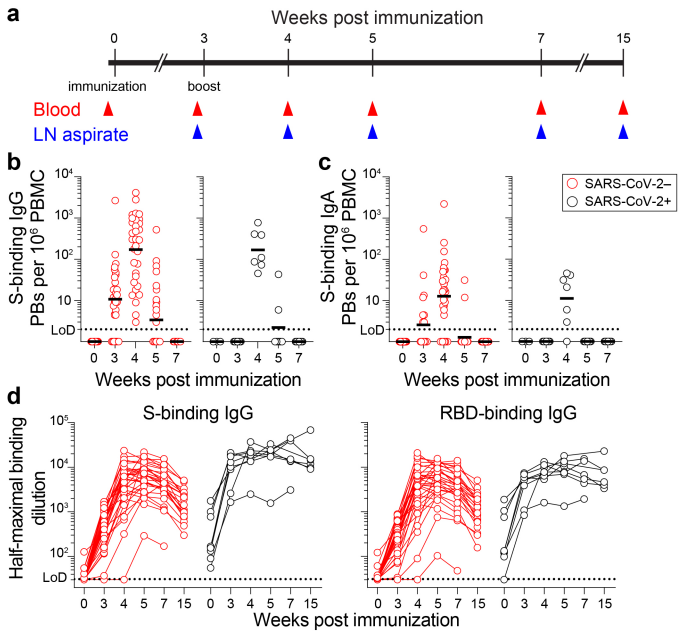


**Figure 1 | Plasmablast and antibody response to SARS-CoV-2 immunization. a**, Study design. Forty-one healthy adult volunteers (ages 28–73, 8 with history of SARS-CoV-2 infection) were enrolled and received BNT162b2 mRNA SARS-CoV-2 vaccine. Blood was collected pre-immunization, and 3, 4, 5, 7, and 15 weeks after immunization. For 14 participants (ages 28–52, none with history of SARS-CoV-2 infection), fine needle aspirates (FNAs) of ipsilateral axillary lymph nodes (LNs) were collected 3, 4, 5, 7, and 15 weeks after immunization. **b, c**, ELISpot quantification of S-binding IgG- (b) and IgA- (c) secreting plasmablasts (PBs) in blood at baseline, 3, 4, 5, and 7 weeks post-immunization in participants without (red) and with (black) history of SARS-CoV-2 infection. **d**, Plasma IgG titers against SARS-CoV-2 spike protein (S) (left) and the receptor binding domain (RBD) of S (right) measured by ELISA in participants without (red) and with (black) history of SARS-CoV-2 infection at baseline, 3, 4, 5, 7, and 15 weeks post-immunization. Dotted lines indicate limits of detection. Symbols at each timepoint in **b**–**d** represent one sample (n= 41). Results are from one experiment performed in duplicate.

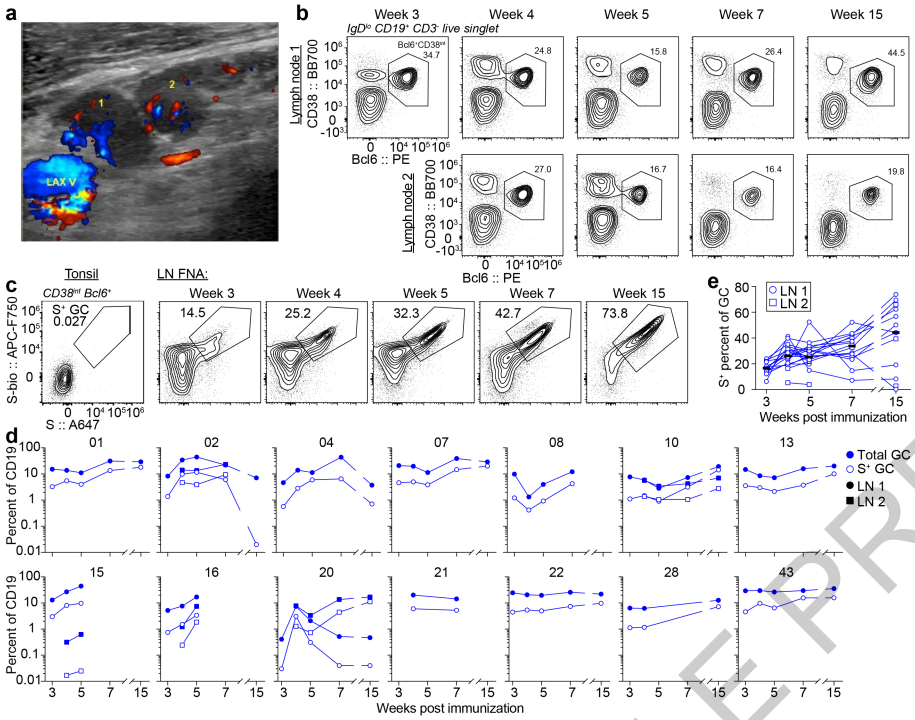


**Figure 2 | Germinal centre B cell response to SARS-CoV-2 immunization.** **a**, Representative color Doppler ultrasound image of two draining LNs "1", and "2" adjacent to the axillary vein "LAX V" 5 weeks after immunization. **b, c**, Representative flow cytometry plots of Bcl6 and CD38 staining on IgD$^{lo}$ CD19$^{+}$ CD3$^{-}$ live singlet lymphocytes in FNA samples (b) and S staining on Bcl6$^{+}$CD38$^{int}$ GC B cells in tonsil and FNA samples (c) at the indicated times after immunization. **d, e**, Kinetics of total (blue) and S$^{+}$ (white) GC B cells as gated in **b** and **c** (d) and S-binding percent of GC B cells (e) from FNA of draining lymph nodes. Symbols at each timepoint represent one FNA sample; square symbols denote second LN sampled (n = 14). Horizontal lines indicate the median.

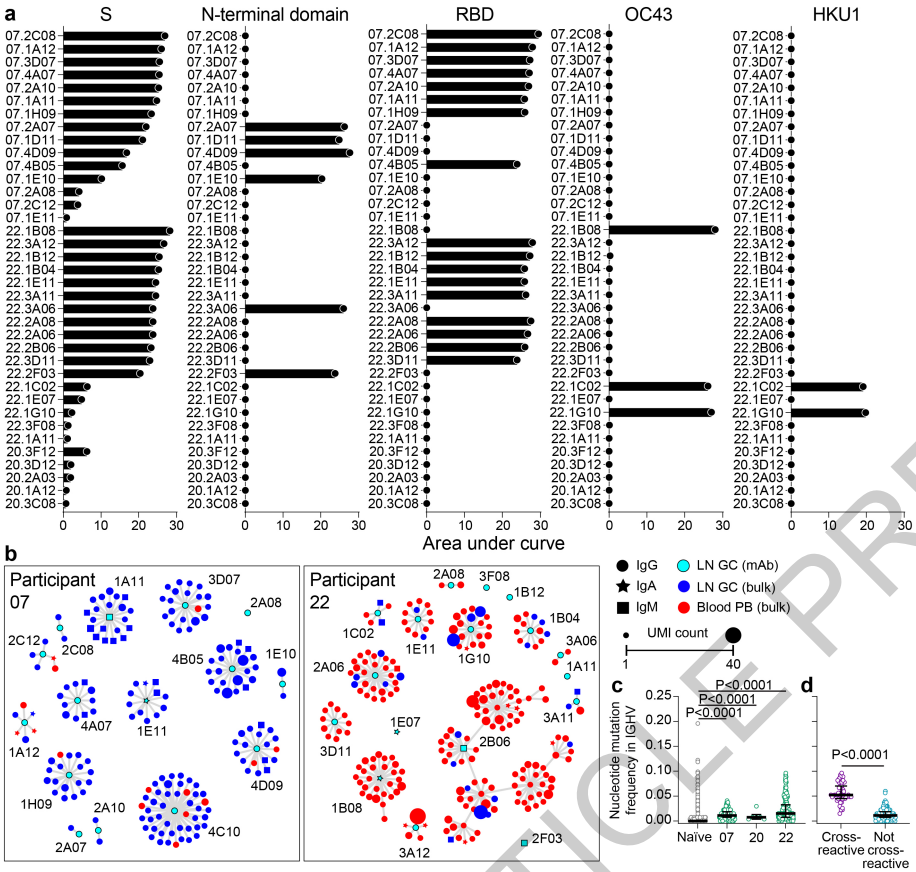


**Figure 3 | Clonal analysis of GC response to SARS-CoV-2 immunization.** **a**, Binding of mAbs generated from GC B cells to SARS-CoV-2 S, N-terminal domain of S, RBD, or spike proteins of betacoronavirus OC43 or HKU1 measured by ELISA. Results are from one experiment performed in duplicate. Baseline for area under the curve was set to the mean + three times the standard deviation of background binding to bovine serum albumin. **b**, Clonal relationship of sequences from S-binding GC mAbs (cyan) to sequences from bulk repertoire analysis of PBs from PBMCs (red) and GC B cells (blue) sorted 4 weeks after immunization. Each clone is visualized as a network in which each node represents a sequence and sequences are linked as a minimum spanning tree of the network. Symbol shape indicates sequence isotype: IgG (circle), IgA (star), and IgM (square); symbol size corresponds to sequence count. **c, d**, Comparison of nucleotide mutation frequency in immunoglobulin heavy chain variable region (*IGHV*) genes of naïve B cells sorted from influenza vaccinees[19] (grey) to clonal relatives of S-binding mAbs among PBs sorted from PBMCs and GC B cells 4 weeks after immunization (green) in indicated participants (c) and between clonal relatives of S-binding mAbs cross-reactive (purple) or not (teal) to seasonal coronavirus spike proteins among PBs sorted from PBMCs and GC B cells 4 weeks after immunization (d). Horizontal lines and error bars indicate the median and interquartile range. Sequence counts were 2,553 (naive), 199 (participant 07), 6 (participant 20), 240 (participant 22), 54 (cross-reactive), and 391 (not cross-reactive). *P* values from two-sided Kruskal–Wallis test with Dunn's post-test between naïve B cells and S-binding clones (c) or two-sided Mann–Whitney U test (d).

# Methods

### Sample collection, preparation, and storage

All studies were approved by the Institutional Review Board of Washington University in St. Louis. Written consent was obtained from all participants. Forty-one healthy volunteers were enrolled, of whom 14 provided axillary LN samples (Extended Data Table 1). In 5 of the 14 participants, a second draining LN was identified and sampled following secondary immunization. One participant (15) received the second immunization in the contralateral arm; draining LNs were identified and sampled on both sides. Blood samples were collected in EDTA tubes, and peripheral blood mononuclear cells (PBMCs) were enriched by density gradient centrifugation over Ficoll 1077 (GE) or Lymphopure (BioLegend). The residual red blood cells were lysed with ammonium chloride lysis buffer, and cells were immediately used or cryopreserved in 10% dimethylsulfoxide in FBS. Ultrasound-guided FNA of axillary LNs was performed by a radiologist or a qualified physician's assistant under the supervision of a radiologist. LN dimensions and cortical thickness were measured, and the presence and degree of cortical vascularity and location of the LN relative to the axillary vein were determined prior to each FNA. For each FNA sample, six passes were made under continuous real-time ultrasound guidance using 25-gauge needles, each of which was flushed with 3 mL of RPMI 1640 supplemented with 10% FBS and 100 U/mL penicillin/streptomycin, followed by three 1-mL rinses. Red blood cells were lysed with ammonium chloride buffer (Lonza), washed with PBS supplemented with 2% FBS and 2 mM EDTA, and immediately used or cryopreserved in 10% dimethylsulfoxide in FBS. Participants reported no adverse effects from phlebotomies or serial FNAs.

### Cell lines

Expi293F cells were cultured in Expi293 Expression Medium (Gibco). Vero E6 (CRL-1586, American Type Culture Collection), Vero-TMPRSS2 cells[38] (a gift from Siyuan Ding, Washington University School of Medicine), and Vero-hACE2-TMPRSS2 (a gift of A. Creanga and B. Graham, National Institutes of Health) cells were cultured at 37 °C in Dulbecco's modified Eagle medium (DMEM) supplemented with 10% fetal bovine serum (FBS), 10 mM HEPES (pH 7.3), 1 mM sodium pyruvate, 1× nonessential amino acids and 100 U ml −1 of penicillin–streptomycin. Vero-TMPRSS2 cell cultures were supplemented with 5 μg ml −1 of blasticidin. Vero-hACE2-TMPRSS2 cell cultures were supplemented with 10 μg ml −1 of puromycin.

### Viruses

The 2019n-CoV/USA_WA1/2020 isolate of SARS-CoV-2 was obtained from the US Centers for Disease Control. The UK B.1.1.7 isolate was obtained from an infected individual. The point mutation D614G in the spike gene was introduced into an infectious complementary DNA clone of the 2019n-CoV/USA_WA1/2020 strain as described previously[39]. Nucleotide substitutions were introduced into a subclone puc57-CoV-2-F5-7 containing the spike gene of the SARS-CoV-2 wild-type infectious clone[40].The South African variant spike gene (B.1.351) was produced synthetically by Gibson assembly. The full-length infectious cDNA clones of the variant SARS-CoV-2 viruses were assembled by *in vitro* ligation of seven contiguous cDNA fragments following a previously described protocol[40]. *In vitro* transcription was then performed to synthesize full-length genomic RNA. To recover the mutant viruses, the RNA transcripts were electroporated into Vero E6 cells. The viruses from the supernatant of cells were collected 40-h later and served as p0 stocks. All viruses were passaged once in Vero-hACE2-TMPRSS2 cells and subjected to deep sequencing after RNA extraction to confirm the introduction and stability of substitutions[17]. All virus preparation and experiments were performed in an approved Biosafety level 3 (BSL-3) facility.

### Antigens

Recombinant soluble SARS-CoV-2 spike (S) protein, recombinant receptor binding domain of S (RBD), human coronavirus OC43 spike, and human coronavirus HKU1 spike were expressed as previously described[41]. Briefly, mammalian cell codon-optimized nucleotide sequences coding for the soluble ectodomain of the spike protein of SARS-CoV-2 (GenBank: MN908947.3, amino acids 1-1213) including a C-terminal thrombin cleavage site, T4 foldon trimerization domain, and hexahistidine tag and for the receptor binding domain (RBD, amino acids 319-541) along with the signal peptide (amino acids 1-14) plus a hexahistidine tag were cloned into mammalian expression vector pCAGGS. The spike protein sequence was modified to remove the polybasic cleavage site (RRAR to A), and two pre-fusion stabilizing proline mutations were introduced (K986P and V987P, wild type numbering). Expression plasmids encoding for the spike of common human coronaviruses OC43 and HKU1 were provided by Barney Graham (Vaccine Research Center, NIH)[42]. Recombinant proteins were produced in Expi293F cells (ThermoFisher) by transfection with purified DNA using the ExpiFectamine 293 Transfection Kit (ThermoFisher). Supernatants from transfected cells were harvested 3 days post-transfection, and recombinant proteins were purified using Ni-NTA agarose (ThermoFisher), then buffer exchanged into phosphate buffered saline (PBS) and concentrated using Amicon Ultracel centrifugal filters (EMD Millipore). For flow cytometry staining, recombinant S was labeled with Alexa Fluor 647-NHS ester or biotinylated using the EZ-Link Micro NHS-PEG4-Biotinylation Kit (Thermo Fisher); excess Alexa Fluor 647 and biotin were removed using 7-kDa Zeba desalting columns (Pierce).

### ELISpot assay

Plates were coated with Flucelvax Quadrivalent 2019/2020 seasonal influenza virus vaccine (Sequiris), S, or RBD. A direct *ex-vivo* ELISpot assay was performed to determine the number of total, vaccine-binding, or recombinant S-binding IgG- and IgA-secreting cells present in PBMC samples using IgG/IgA double-color ELISpot Kits (Cellular Technology Limited) according to the manufacturer's instructions. ELISpot plates were analyzed using an ELISpot counter (Cellular Technology Limited).

### ELISA

Assays were performed in 96-well plates (MaxiSorp; Thermo) coated with 100 μL of recombinant S, RBD, N-terminal domain of S (SinoBiological), OC43 spike, HKU1 spike, or bovine serum albumin diluted to 1 μg/mL in PBS, and plates were incubated at 4 °C overnight. Plates then were blocked with 10% FBS and 0.05% Tween 20 in PBS. Plasma or purified mAbs were serially diluted in blocking buffer and added to the plates. Plates were incubated for 90 min at room temperature and then washed 3 times with 0.05% Tween 20 in PBS. Goat anti-human IgG-HRP (goat polyclonal, Jackson ImmunoResearch, 1:2,500), IgA (goat polyclonal, Jackson ImmuoResearch, 1:2500), or IgM (goat polyclonal, Caltag, 1:4000) were diluted in blocking buffer before adding to wells and incubating for 60 min at room temperature. Plates were washed 3 times with 0.05% Tween 20 in PBS and 3 times with PBS before the addition of o-phenylenediamine dihydrochloride peroxidase substrate (Sigma-Aldrich). Reactions were stopped by the addition of 1 M hydrochloric acid. Optical density measurements were taken at 490 nm. The area under the curve for each mAb and half-maximal binding dilution for each plasma sample were calculated using Graphpad Prism v8.

### Focus reduction neutralization test

Plasma samples were declotted by diluting 1:10 in DMEM supplemented with 2% FBS, 10 mM HEPES, and 100 U/mL penicillin/streptomycin and incubating for 3 h at 37 °C. Serial dilutions of resulting serum were incubated with $10^2$ focus-forming units of different strains or variants of SARS-CoV-2 for 1 h at 37 °C. Antibody-virus complexes were added to Vero-TMPRSS2 cell monolayers in 96-well plates and incubated at

37 °C for 1 h. Subsequently, cells were overlaid with 1% (w/v) methylcellulose in MEM supplemented with 2% FBS. Plates were harvested 30 h later by removing overlays and fixed with 4% PFA in PBS for 20 min at room temperature. Plates were washed and sequentially incubated with an oligoclonal pool of murine anti-S mAbs (SARS2-2, SARS2-11, SARS2-16, SARS2-31, SARS2-38, SARS2-57, and SARS2-71) (ref. [43]) and HRP-conjugated goat anti-mouse IgG (polyclonal, Sigma, 1:500) in PBS supplemented with 0.1% saponin and 0.1% bovine serum albumin. SARS-CoV-2-infected cell foci were visualized using TrueBlue peroxidase substrate (KPL) and quantitated on an ImmunoSpot microanalyzer (Cellular Technology Limited).

### Cell sorting and flow cytometry

Staining for flow cytometry analysis and sorting was performed using freshly isolated or cryo-preserved FNA, PBMC, or tonsil samples. For analysis, cells were incubated for 30 min on ice with biotinylated and Alexa Fluor 647 conjugated recombinant soluble S and PD-1-BB515 (EH12.1, BD Horizon, 1:100) in 2% FBS and 2 mM EDTA in PBS (P2), washed twice, then stained for 30 min on ice with IgG-BV480 (goat polyclonal, Jackson ImmunoResearch, 1:100), IgA-FITC (M24A, Millipore, 1:500), CD45-A532 (HI30, Thermo, 1:50), CD38-BB700 (HIT2, BD Horizon, 1:500), CD20-Pacific Blue (2H7, 1:400), CD27-BV510 (O323, 1:50), CD8-BV570 (RPA-T8, 1:200), IgM-BV605 (MHM-88, 1:100), HLA-DR-BV650 (L243, 1:100), CD19-BV750 (HIB19, 1:100), CXCR5-PE-Dazzle 594 (J252D4, 1:50), IgD-PE-Cy5 (IA6-2, 1:200), CD14-PerCP (HCD14, 1:50), CD71-PE-Cy7 (CY1G4, 1:400), CD4-Spark685 (SK3, 1:200), streptavidin-APC-Fire750, CD3-APC-Fire810 (SK7, 1:50), and Zombie NIR (all BioLegend) diluted in Brilliant Staining buffer (BD Horizon). Cells were washed twice with P2, fixed for 1 h at 25 °C using the True Nuclear fixation kit (BioLegend), washed twice with True Nuclear Permeabilization/Wash buffer, stained with FoxP3-BV421 (206D, BioLegend, 1:15), Ki-67-BV711 (Ki-67, BioLegend, 1:200), Tbet-BV785 (4B10, BioLegend, 1:400), Bcl6-PE (K112-91, BD Pharmingen, 1:25), and Blimp1-A700 (646702, R&D, 1:50) for 1h at 25 °C, washed twice with True Nuclear Permeabilization/Wash buffer, and acquired on an Aurora using SpectroFlo v2.2 (Cytek). Flow cytometry data were analyzed using FlowJo v10 (Treestar).

For sorting GC B cells, FNA single cell suspensions were stained for 30 min on ice with CD19-BV421 (HIB19, 1:100), CD3-FITC (HIT3a, 1:200), IgD-PerCP-Cy5.5 (IA6-2, 1:200), CD71-PE (CY1G4, 1:400), CXCR5-PE-Dazzle 594 (J252D4, 1:50), CD38-PE-Cy7 (HIT2, 1:200), CD20-APC-Fire750 (2H7, 1:100), Zombie Aqua (all BioLegend), and Alexa Fluor 647 conjugated recombinant soluble S. For sorting plasmablasts, PBMCs were stained for 30 min on ice with CD20-PB (2H7, 1:400), CD71-FITC (CY1G4, 1:200), CD4-PerCP (OKT4, 1:100), IgD-PE (IA6-2, 1:200), CD38-PE-Cy7 (HIT2, 1:200), CD19-APC (HIB19, 1:200), and Zombie Aqua (all BioLegend). Cells were washed twice, and single S-binding GC B cells (live singlet $CD3^-$ $CD19^+$ $IgD^{lo}$ $CD20^{hi}$ $CD38^{int}$ $CD71^+$ $CXCR5^+$ $S^+$) were sorted using a FACSAria II into 96-well plates containing 2 µL Lysis Buffer (Clontech) supplemented with 1 U/µL RNase inhibitor (NEB), or total GC B cells or plasmablasts (live singlet $CD3^-$ $CD19^+$ $IgD^{lo}$ $CD20^{lo}$ $CD38^+$ $CD71^+$) were bulk sorted into buffer RLT Plus (Qiagen) and immediately frozen on dry ice.

### Monoclonal antibody (mAb) generation

Antibodies were cloned as described previously[44]. Briefly, VH, Vκ, and Vλ genes were amplified by reverse transcription-PCR and nested PCR reactions from singly-sorted GC B cells using primer combinations specific for IgG, IgM/A, Igκ, and Igλ from previously described primer sets[45] and then sequenced. To generate recombinant antibodies, restriction sites were incorporated via PCR with primers to the corresponding heavy and light chain V and J genes. The amplified VH, Vκ, and Vλ genes were cloned into IgG1 and Igκ or Igλ expression vectors, respectively, as described previously[45–47]. Heavy and light chain plasmids were co-transfected into Expi293F cells (Gibco) for expression, and antibody was purified using protein A agarose chromatography (Goldbio). Sequences were obtained from PCR reaction products and annotated using the ImMunoGeneTics (IMGT)/V-QUEST database (http://www.imgt.org/IMGT_vquest/)[48,49]. Mutation frequency was calculated by counting the number of nonsynonymous nucleotide mismatches from the germline sequence in the heavy chain variable segment leading up to the CDR3, while excluding the 5′ primer sequences that could be error-prone.

### Bulk BCR sequencing

RNA was purified from sorted PBs from PBMCs and GC B cells from LNs from participants 07, 20 (LN 1), and 22 using the RNeasy Plus Micro kit (Qiagen). Reverse transcription, unique molecular identifier (UMI) barcoding, cDNA amplification, and Illumina linker addition to B cell heavy chain transcripts were performed using the human NEBNext Immune Sequencing Kit (New England Biolabs) according to the manufacturer's instructions. High-throughput 2x300bp paired-end sequencing was performed on the Illumina MiSeq platform with a 30% PhiX spike-in according to manufacturer's recommendations, except for performing 325 cycles for read 1 and 275 cycles for read 2.

### Processing of BCR bulk sequencing reads

Demultiplexed pair-end reads were BLAST'ed using blastn v2.11.0 (ref. [50]) for PhiX removal and subsequently preprocessed using pRESTO v0.6.2 (ref. [51]) as follows. 1) Reads with a mean *Phred* quality score below 20 were filtered. 2) Reads were aligned against template switch sequences and constant region primers (Extended Data Table 5), with a maximum mismatch rate of 0.5 and 0.2 respectively. 3) A UMI was assigned to each read by extracting the first 17 nucleotides preceding the template switch site. 4) Sequencing and multiplexing errors in the UMI region were then corrected using the approach described in Jiang et al[52]. Briefly, reads with similar UMIs were clustered using cd-hit-est v4.8.1 (ref. [53]) based on the pairwise distance of their UMIs with a similarity threshold of 0.83 that was estimated from 10,000 reads. The UMI-based read groups were further clustered within themselves based on the pairwise distance of the non-UMI region of their reads with a similarity threshold of 0.8. Read clusters spanning multiple multiplexed samples were assigned to the majority sample. 5) Separate consensus sequences for the forward and reverse reads within each read cluster were constructed with a maximum error score of 0.1 and minimum constant region primer frequency of 0.6. If multiple constant region primers were associated with a particular read cluster, the majority primer was used. 6) Forward and reverse consensus sequence pairs were assembled by first attempting *de novo* assembly with a minimum overlap of 8 nucleotides and a maximum mismatch rate of 0.3. If unsuccessful, this was followed by reference-guided assembly using blastn v2.11.0 (ref. [50]) with a minimum identity of 0.5 and an E-value threshold of $1*10^{-5}$. 7) Isotypes were assigned by local alignment of the 3′ end of each consensus sequence to isotype-specific internal constant region sequences with a maximum mismatch rate of 0.3. Sequences with inconsistent isotype assignment and constant region primer alignment were removed. 8) Duplicate consensus sequences, except those with different isotype assignments, were collapsed into unique sequences. Only unique consensus sequences with at least two contributing reads were used subsequently (Extended Data Table 6).

### BCR genotyping

Initial germline V(D)J gene annotation was performed using IgBLAST v1.17.1 (ref. [54]) with IMGT/GENE-DB release 202113-2 (ref. [55]). IgBLAST output was parsed using Change-O v1.0.2 (ref. [56]). Quality control was performed, requiring each sequence to have non-empty V and J gene annotations; exhibit chain consistency in all annotations; bear fewer than 10 non-informative (non-A/T/G/C, such as N or -) positions; and carry a CDR3 with no N and a nucleotide length that is a multiple of 3. Individualized genotypes were inferred using TIgGER v1.0.0

(ref. [57]) and used to finalize V(D)J annotations. Sequences annotated as non-productively rearranged by IgBLAST were removed from further analysis.

### Clonal lineage analysis

B cell clonal lineages were inferred based on productively rearranged heavy chain sequences using hierarchical clustering with single linkage[58,59]. Sequences were first partitioned based on common V and J gene annotations and CDR3 lengths. Within each partition, sequences whose CDR3s were within 0.15 normalized Hamming distance from each other were clustered as clones. This distance threshold was determined by manual inspection in conjunction with kernel density estimates, in order to identify the local minimum between the two modes of the within-participant bimodal distance-to-nearest distribution (Extended Data Fig. 1d). Following clonal clustering, full-length clonal consensus germline sequences were reconstructed for each clone with D-segment and N/P regions masked with N's, resolving any ambiguous gene assignments by majority rule. Within each clone, duplicate IMGT-aligned V(D)J sequences from bulk sequencing were collapsed with the exception of duplicates derived from different B cell compartments or isotypes. Clones were visualized as networks[60] using igraph v1.2.5 (ref. [61]). First, a full network was calculated for each clone, in which an edge was drawn between every pair of sequences whose CDR3s were within 0.15 normalized Hamming distance from each other. Then, a minimum spanning tree (MST) was derived from the full network, in which only edges essential for ensuring that all sequences connected in the full network remain connected in the MST either directly or indirectly were retained. The MST was then visualized for each clone.

### Calculation of SHM frequency

Mutation frequency was calculated by counting the number of nucleotide mismatches from the germline sequence in the observed heavy chain variable segment leading up to the CDR3, while excluding the first 18 positions that could be error-prone due to the primers used for generating the mAb sequences. Calculation was performed using the calcObservedMutations function from SHazaM v1.0.2 (ref. [56]).

### Reporting summary

Further information on research design is available in the Nature Research Reporting Summary linked to this paper.

## Data availability

Antibody sequences are deposited on GenBank under the following accession numbers: MW926396–MW926407, MW926409–MW926430, MW926432–MW926441, MZ292481–MZ292510, available from GenBank/EMBL/DDBJ. Bulk sequencing reads are deposited on Sequence Read Archive under BioProject PRJNA731610. The IMGT/V-QUEST database is accessible at http://www.imgt.org/IMGT_vquest/. Other relevant data are available from the corresponding author upon request.


38. Zang, R. *et al*. TMPRSS2 and TMPRSS4 promote SARS-CoV-2 infection of human small intestinal enterocytes. *Sci. Immunol*. **5**, eabc3582 (2020).
39. Plante, J. A. *et al*. Spike mutation D614G alters SARS-CoV-2 fitness. *Nature* (2020) https://doi.org/10.1038/s41586-020-2895-3.
40. Xie, X. *et al*. An Infectious cDNA Clone of SARS-CoV-2. *Cell Host Microbe* **27**, 841-848.e3 (2020).
41. Stadlbauer, D. *et al*. SARS-CoV-2 Seroconversion in Humans: A Detailed Protocol for a Serological Assay, Antigen Production, and Test Setup. *Curr. Protoc. Microbiol*. **57**, (2020).
42. Pallesen, J. *et al*. Immunogenicity and structures of a rationally designed prefusion MERS-CoV spike antigen. *Proc. Natl. Acad. Sci*. **114**, E7348–E7357 (2017).
43. Liu, Z. *et al*. Identification of SARS-CoV-2 spike mutations that attenuate monoclonal and serum antibody neutralization. *Cell Host Microbe* S1931312821000445 (2021) https://doi.org/10.1016/j.chom.2021.01.014
44. Wrammert, J. *et al*. Broadly cross-reactive antibodies dominate the human B cell response against 2009 pandemic H1N1 influenza virus infection. *J. Exp. Med*. **208**, 181–193 (2011).
45. Smith, K. *et al*. Rapid generation of fully human monoclonal antibodies specific to a vaccinating antigen. *Nat. Protoc*. **4**, 372–384 (2009).
46. Wrammert, J. *et al*. Rapid cloning of high-affinity human monoclonal antibodies against influenza virus. *Nature* **453**, 667–671 (2008).
47. Nachbagauer, R. *et al*. Broadly Reactive Human Monoclonal Antibodies Elicited following Pandemic H1N1 Influenza Virus Exposure Protect Mice against Highly Pathogenic H5N1 Challenge. *J. Virol*. **92**, 1–17 (2018).
48. Brochet, X., Lefranc, M.-P. & Giudicelli, V. IMGT/V-QUEST: the highly customized and integrated system for IG and TR standardized V-J and V-D-J sequence analysis. *Nucleic Acids Res*. **36**, W503–W508 (2008).
49. Giudicelli, V., Brochet, X. & Lefranc, M.-P. IMGT/V-QUEST: IMGT Standardized Analysis of the Immunoglobulin (IG) and T Cell Receptor (TR) Nucleotide Sequences. *Cold Spring Harb. Protoc*. **2011**, pdb.prot5633-pdb.prot5633 (2011).
50. Camacho, C. *et al*. BLAST+: Architecture and applications. *BMC Bioinformatics* **10**, 1–9 (2009).
51. Vander Heiden, J. A. *et al*. PRESTO: A toolkit for processing high-throughput sequencing raw reads of lymphocyte receptor repertoires. *Bioinformatics* **30**, 1930–1932 (2014).
52. Jiang, R. *et al*. Thymus-derived B cell clones persist in the circulation after thymectomy in myasthenia gravis. *Proc. Natl. Acad. Sci*. **117**, 30649–30660 (2020).
53. Li, W. & Godzik, A. Cd-hit: a fast program for clustering and comparing large sets of protein or nucleotide sequences. *Bioinformatics* **22**, 1658–1659 (2006).
54. Ye, J., Ma, N., Madden, T. L. & Ostell, J. M. IgBLAST: an immunoglobulin variable domain sequence analysis tool. *Nucleic Acids Res*. **41**, W34–W40 (2013).
55. Giudicelli, V., Chaume, D. & Lefranc, M. P. IMGT/GENE-DB: A comprehensive database for human and mouse immunoglobulin and T cell receptor genes. *Nucleic Acids Res*. **33**, 256–261 (2005).
56. Gupta, N. T. *et al*. Change-O: A toolkit for analyzing large-scale B cell immunoglobulin repertoire sequencing data. *Bioinformatics* **31**, 3356–3358 (2015).
57. Gadala-Maria, D., Yaari, G., Uduman, M. & Kleinstein, S. H. Automated analysis of high-throughput B-cell sequencing data reveals a high frequency of novel immunoglobulin V gene segment alleles. *Proc. Natl. Acad. Sci. U. S. A*. **112**, E862–E870 (2015).
58. Gupta, N. T. *et al*. Hierarchical Clustering Can Identify B Cell Clones with High Confidence in Ig Repertoire Sequencing Data. *J. Immunol*. **198**, 2489–2499 (2017).
59. Zhou, J. Q. & Kleinstein, S. H. Cutting Edge: Ig H Chains Are Sufficient to Determine Most B Cell Clonal Relationships. *J. Immunol*. **203**, 1687–1692 (2019).
60. Bashford-Rogers, R. J. M. *et al*. Network properties derived from deep sequencing of human B-cell receptor repertoires delineate B-cell populations. *Genome Res*. **23**, 1874–1884 (2013).
61. Csardi, G. & Nepusz, T. The igraph software package for complex network research. *InterJournal Complex Syst*. **1695**, 1–9 (2006).



**Acknowledgements** We thank the generous participation of the donors for providing specimens. We thank Lisa Kessels, AJ Winingham, Khatira Safi, and the staff of the Infectious Diseases Clinical Research Unit at Washington University School of Medicine for assistance with scheduling participants and sample collection. The Vero-TMPRSS2 cells were kindly provided by Siyuan Ding (Washington University School of Medicine). The expression plasmids encoding for the spike of coronaviruses OC43 and HKU1 were kindly provided by Kizzmekia Corbett and Barney Graham (Vaccine Research Center, NIH). The Ellebedy laboratory was supported by National Institute of Allergy and Infectious Diseases (NIAID) grants U01AI141990 and 1U01AI150747 and NIAID Centers of Excellence for Influenza Research and Surveillance (CEIRS) contract HHSN272201400006C. The Ellebedy and Krammer laboratories were supported by NIAID CEIRS contract HHSN272201400008C and NIAID Collaborative Influenza Vaccine Innovation Centers contract 75N93019C00051. The Diamond laboratory was supported by R01 AI157155. The Shi laboratory was supported by NIH grants AI134907 and UL1TR001439, and awards from the Sealy & Smith Foundation, Kleberg Foundation, the John S. Dunn Foundation, the Amon G. Carter Foundation, the Gilson Longenbaugh Foundation, and the Summerfield Robert Foundation. J.S.T. was supported by NIAID 5T32CA009547. J.B.C. was supported by a Helen Hay Whitney Foundation postdoctoral fellowship. The WU368 study was reviewed and approved by the Washington University Institutional Review Board (approval no. 202012081).


**Author contributions** A.H.E., J.A.O and R.M.P. conceived and designed the study. J.A.O., A.H., M.K.K., and R.M.P. wrote and maintained the IRB protocol, recruited, and phlebotomized participants and coordinated sample collection. J.S.T., E.K., W.K., A.J.S., and T.L. processed specimens. J.S.T., E.K., W.K., and A.J.S. performed ELISA and ELISpot. R.E.C. and J.B.C. performed neutralization assays. J.S.T., E.K., W.K., A.J.S., T.L., and M.T. generated and characterized monoclonal antibodies. A.J.S. performed RNA extractions and library preparation for BCR bulk sequencing. J.Q.Z. analyzed BCR repertoire data. T.S. and W.D.M performed FNA. W.D.M. and S.A.T. supervised lymph node evaluation prior to FNA and specimen collection and evaluated lymph node ultrasound data. A.J.S. expressed SARS-CoV-2 S and RBD proteins. F.A. and F.K. expressed CoV S proteins. J.S.T. sorted cells and collected and analysed the flow cytometry data. X.X. and P.-Y.S. prepared the SARS-CoV-2 with variant spike mutations. J.S.T., A.M.R., and A.H.E. analyzed the data. M.S.D. and A.H.E. supervised experiments and obtained funding. J.S.T. and A.H.E. composed the manuscript. All authors reviewed the manuscript.

**Competing interests** The Ellebedy laboratory received funding under sponsored research agreements that are unrelated to the data presented in the current study from Emergent BioSolutions and from AbbVie. A.H.E. is a consultant for Mubadala Investment Company and the founder of ImmuneBio Consulting. J.S.T., A.J.S., M.S.D., and A.H.E. are recipients of a licensing agreement with Abbvie that is unrelated to the data presented in the current study. M.S.D. is a consultant for Inbios, Vir Biotechnology, Fortress Biotech, and Carnival Corporation, and on the Scientific Advisory Boards of Moderna and Immunome. The Diamond laboratory has received unrelated funding support in sponsored research agreements from Moderna, Vir Biotechnology, and Emergent BioSolutions. A patent application related to this work has been filed by Washington University School of Medicine. The Icahn School of Medicine at Mount Sinai has filed patent applications relating to SARS-CoV-2 serological assays and NDV-based

SARS-CoV-2 vaccines which list Florian Krammer as co-inventor. Mount Sinai has spun out a company, Kantaro, to market serological tests for SARS-CoV-2. Florian Krammer has consulted for Merck and Pfizer (before 2020), and is currently consulting for Pfizer, Seqirus and Avimex. The Krammer laboratory is also collaborating with Pfizer on animal models of SARS-CoV-2. The Shi laboratory has received sponsored research agreements from Pfizer, Gilead, Merck and IGM Sciences Inc. The content of this manuscript is solely the responsibility of the authors and does not necessarily represent the official view of NIAID or NIH.

**Additional information**
**Supplementary information** The online version contains supplementary material available at https://doi.org/10.1038/s41586-021-03738-2.
**Correspondence and requests for materials** should be addressed to R.M.P. or A.H.E.
**Peer review information** *Nature* thanks the anonymous reviewers for their contribution to the peer review of this work. Peer reviewer reports are available.
**Reprints and permissions information** is available at http://www.nature.com/reprints.

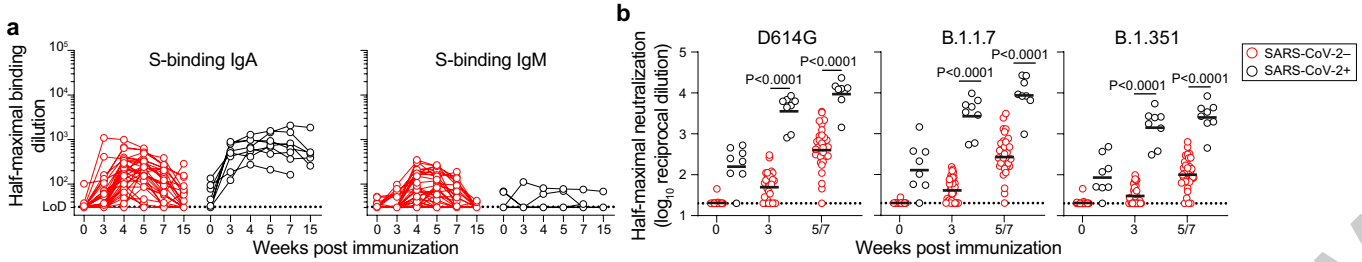


**Extended Data Figure 1 | Antibody response to SARS-CoV-2 immunization.** **a**, Plasma IgA (left) and IgM (right) titers against SARS-CoV-2 spike protein (S) measured by ELISA in participants without (red) and with (black) history of SARS-CoV-2 infection at baseline, 3, 4, 5, 7, and 15 weeks post-immunization. **b**, Neutralizing activity of serum against WA1/2020 D614G (left), B.1.1.7 (middle), and a chimeric virus expressing B.1.351 spike (right) in Vero-TMPRSS2 cells at baseline, 3, and 5 or 7 weeks post-immunization in participants without (red) and with (black) history of SARS-CoV-2 infection. *P* values from two-sided Mann-Whitney tests. Dotted lines indicate limits of detection. Horizontal lines indicate the geometric mean. Symbols at each timepoint represent one sample (n= 41). Results are from one experiment performed in duplicate.

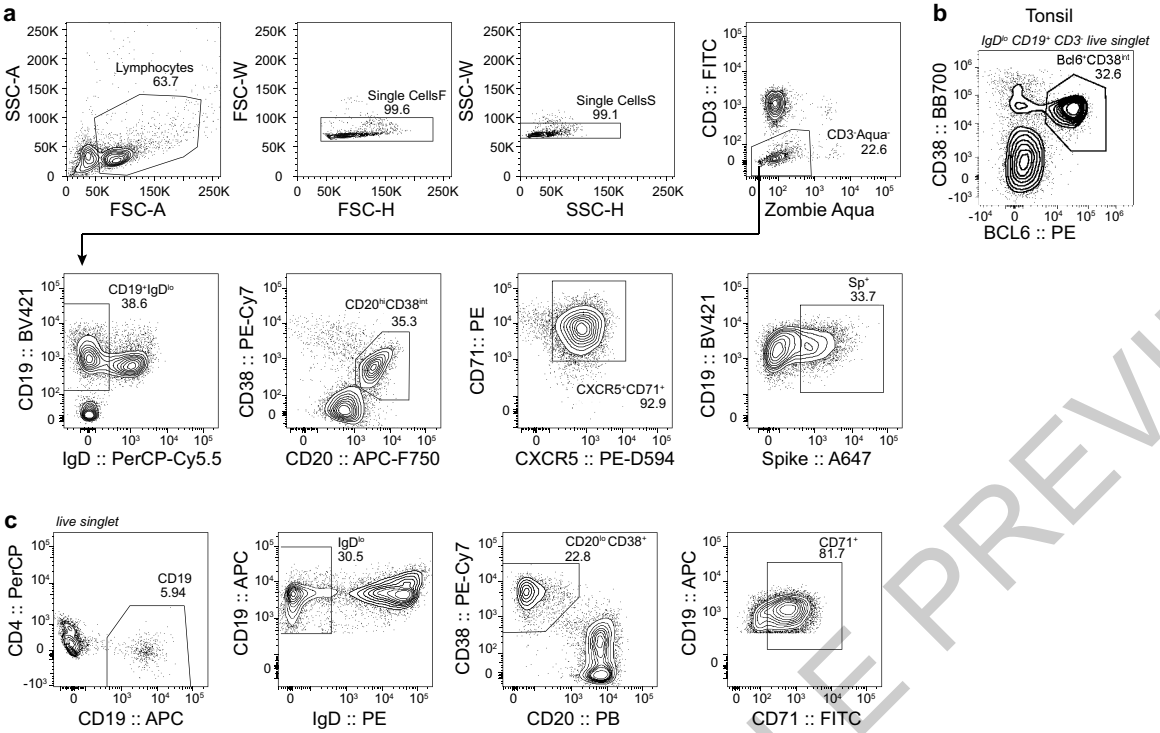


**Extended Data Figure 2 | Gating strategies for analysis of GC response to SARS-CoV-2 immunization. a, c**, Sorting gating strategies for S-binding GC B cells from FNAs (a) and total PBs from PBMCs (c). **b**, Representative plot of GC B cells in tonsil.

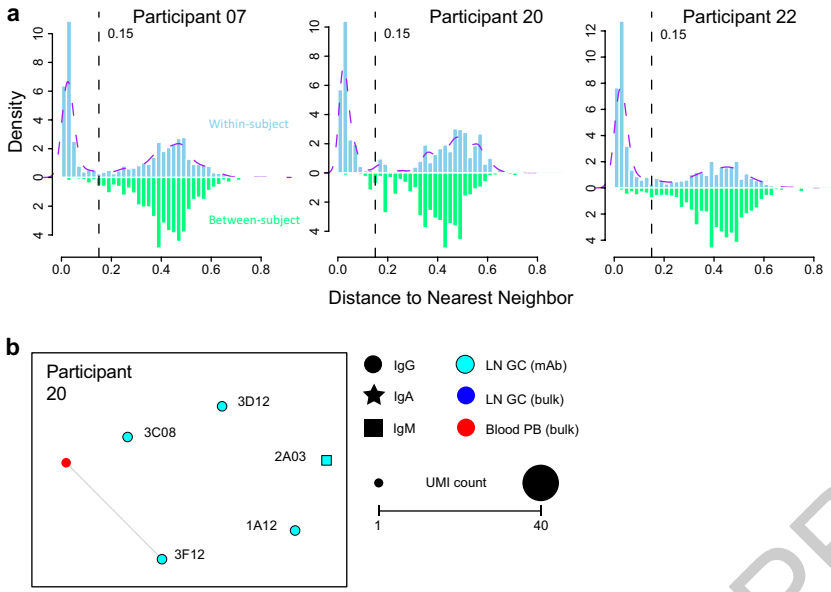


**Extended Data Figure 3 | Clonal analysis of GC response to SARS-CoV-2 immunization. a**, Distance-to-nearest-neighbor plots for choosing a distance threshold for inferring clones via hierarchical clustering. After partitioning sequences based on common V and J genes and CDR3 length, the nucleotide Hamming distance of a CDR3 to its nearest non-identical neighbor from the same participant within its partition was calculated and normalized by CDR3 length (blue histogram). For reference, the distance to the nearest non-identical neighbor from other participants was calculated (green histogram). A clustering threshold of 0.15 (dashed black line) was chosen via manual inspection and kernel density estimate (dashed purple line) to separate the two modes of the within-participant distance distribution representing, respectively, sequences that were likely clonally related and unrelated. **b**, Clonal relationship of sequences from S-binding GC mAbs (cyan) to sequences from bulk repertoire analysis of PBs sorted from PBMCs (red) 4 weeks after immunization. Each clone is visualized as a network in which each node represents a sequence and sequences are linked as a minimum spanning tree of the network. Symbol shape indicates sequence isotype: IgG (circle), IgA (star), and IgM (square); symbol size corresponds to sequence count.

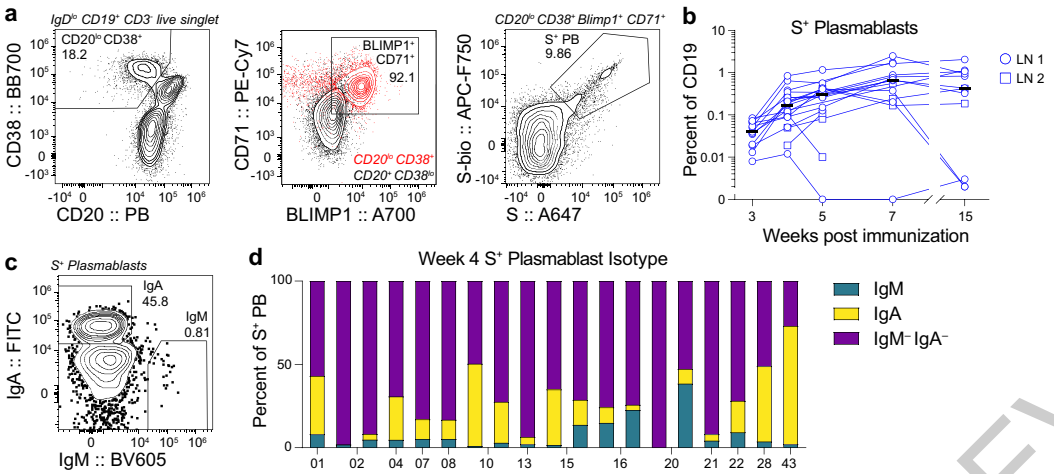


**Extended Data Figure 4 | Lymph node plasmablast response to SARS-CoV-2 immunization. a, c**, Representative flow cytometry plots showing gating of $CD20^{lo}$ $CD38^{+}$ $CD71^{+}$ $Blimp1^{+}$ $S^{+}$ PBs from $IgD^{lo}$ $CD19^{+}$ $CD3^{-}$ live singlet lymphocytes (a) and IgA and IgM staining on $S^{+}$ PBs (c) in FNA samples. **b**, Kinetics of $S^{+}$ PBs gated as in **a** from FNA of draining lymph nodes. Symbols at each timepoint represent one FNA sample; square symbols denote second LN sampled (n = 14). Horizontal lines indicate the median. **d**, Percentages of $IgM^{+}$ (teal), $IgA^{+}$ (yellow), or $IgM^{-}IgA^{-}$ (purple) $S^{+}$ PBs gated as in **c** in FNA of draining LNs 4 weeks after primary immunization. Each bar represents one sample (n = 14).

**Extended Data Table 1 | Participant demographics**

| Variable | Total N=41<br>N (%) | Lymph node N=14<br>N (%) |
|---|---|---|
| **Age (median [range])** | 37 (28-73) | 37 (28-52) |
| **Sex** | | |
| Female | 18 (43.9) | 8 (57.1) |
| Male | 23 (56.1) | 6 (42.9) |
| **Race** | | |
| White | 30 (73.2) | 11 (78.6) |
| Asian | 9 (22) | 2 (14.3) |
| Black | 1 (2.4) | 1 (7.1) |
| Other | 1 (2.4) | 0 (0) |
| **Ethnicity** | | |
| Not of Hispanic, Latinx, or Spanish origin | 39 (95.1) | 13 (92.9) |
| Hispanic, Latinx, Spanish origin | 2 (4.9) | 1 (7.1) |
| **BMI (median [range])** | 25.4 (21.4-40) | 23.9 (21.4-40) |
| **Comorbidities** | | |
| Lung disease | 2 (4.9) | 1 (7.1) |
| Diabetes mellitus | 0 (0) | 0 (0) |
| Hypertension | 7 (17.1) | 2 (14.3) |
| Cardiovascular | 0 (0) | 0 (0) |
| Liver disease | 0 (0) | 0 (0) |
| Chronic kidney disease | 0 (0) | 0 (0) |
| Cancer on chemotherapy | 0 (0) | 0 (0) |
| Hematological malignancy | 0 (0) | 0 (0) |
| Pregnancy | 0 (0) | 0 (0) |
| Neurological | 0 (0) | 0 (0) |
| HIV | 0 (0) | 0 (0) |
| Solid organ transplant recipient | 0 (0) | 0 (0) |
| Bone marrow transplant recipient | 0 (0) | 0 (0) |
| Hyperlipidemia | 1 (2.4) | 0 (0) |
| **Confirmed SARS-CoV-2 infection** | 8 (19.5) | 0 (0) |
| Time from SARS-CoV-2 infection to baseline visit in days (median [range]) | 122 (50-307) | -- |

**Extended Data Table 2 | Vaccine side effects**

| Variable | Total N=41<br>N (%) | | Total N=41<br>N (%) |
|---|---|---|---|
| **First dose** | | **Second dose** | |
| None | 3 (7.3) | None | 1 (2.4) |
| Chills | 5 (12.2) | Chills | 15 (36.6) |
| Fever | 2 (4.9) | Fever | 6 (14.6) |
| Headache | 6 (14.6) | Headache | 11 (26.8) |
| Injection site pain | 33 (80.5) | Injection site pain | 36 (87.8) |
| Muscle or joint pain | 9 (21.9) | Muscle or joint pain | 32 (78) |
| Fatigue | 8 (19.5) | Fatigue | 23 (56.1) |
| Sweating | 0 (0) | Sweating | 2 (4.8) |
| | **Duration of side effects in hours (median [range])** | | |
| Chills | 48 (6-72) | Chills | 24 (4-48) |
| Fever | 9 (6-12) | Fever | 24 (1-48) |
| Headache | 9 (3-48) | Headache | 24 (4-48) |
| Injection site pain | 36 (2-120) | Injection site pain | 36 (2-120) |
| Muscle or joint pain | 36 (1-48) | Muscle or joint pain | 24 (1-48) |
| Fatigue | 30 (3-48) | Fatigue | 24 (3-144) |
| Sweating | 0 (0) | Sweating | 18 (18) |

**Extended Data Table 3 | Lymph node population frequencies**

| Participant | Week post immunization | LN # | Total GC (%CD19) | S+ GC (%CD19) | S+ PB (%CD19) | CD14 (%live singlet) |
|---|---|---|---|---|---|---|
| 01 | 3 | 1 | 15.1744 | 3.2617 | 0.0718 | 0.2134 |
| 01 | 4 | 1 | 13.7195 | 5.4700 | 0.8436 | 0.0588 |
| 01 | 5 | 1 | 11.1280 | 4.0445 | 1.1611 | 0.1461 |
| 01 | 7 | 1 | 31.1819 | 13.5866 | 1.6436 | 0.1469 |
| 01 | 15 | 1 | 29.0930 | 18.1334 | 2.0446 | 0.1628 |
| 02 | 3 | 1 | 8.2782 | 1.3827 | 0.0132 | 0.1590 |
| 02 | 4 | 1 | 34.1504 | 9.7890 | 0.2102 | 0.1705 |
| 02 | 4 | 2 | 14.0743 | 4.7121 | 0.2521 | 0.1371 |
| 02 | 5 | 1 | 44.6608 | 11.6465 | 0.4086 | 0.0743 |
| 02 | 5 | 2 | 13.5353 | 3.8936 | 0.2893 | 0.1361 |
| 02 | 7 | 1 | 21.8959 | 6.0492 | 0.3725 | 0.2486 |
| 02 | 7 | 2 | 23.1123 | 9.3883 | 0.5557 | 0.7063 |
| 02 | 15 | 1 | 7.1063 | 0.0197 | 0.0020 | 0.1649 |
| 04 | 3 | 1 | 4.6727 | 0.5706 | 0.0538 | 0.1934 |
| 04 | 4 | 1 | 13.9308 | 2.8621 | 0.0885 | 0.3733 |
| 04 | 5 | 1 | 11.3856 | 5.9721 | 0.4296 | 0.7237 |
| 04 | 7 | 1 | 43.8266 | 6.4556 | 0.2019 | 0.1436 |
| 04 | 15 | 1 | 3.7193 | 0.7127 | 0.0025 | 0.9901 |
| 07 | 3 | 1 | 21.0403 | 4.6411 | 0.0697 | 0.1927 |
| 07 | 4 | 1 | 19.6634 | 4.9771 | 0.2599 | 0.1507 |
| 07 | 5 | 1 | 11.3504 | 3.8557 | 0.2576 | 0.4177 |
| 07 | 7 | 1 | 39.2049 | 14.7032 | 0.6765 | 0.6582 |
| 07 | 15 | 1 | 28.9957 | 20.1221 | 0.3248 | 0.0349 |
| 08 | 3 | 1 | 9.9010 | 1.2181 | 0.0651 | 0.2738 |
| 08 | 4 | 1 | 1.3233 | 0.4150 | 0.0904 | 0.1670 |
| 08 | 5 | 1 | 3.9913 | 0.9238 | 0.1507 | 0.3377 |
| 08 | 7 | 1 | 12.1411 | 4.2393 | 0.7559 | 0.8097 |
| 10 | 3 | 1 | 7.7130 | 1.1146 | 0.0399 | 0.2216 |
| 10 | 4 | 1 | 5.9172 | 1.4892 | 0.3494 | 0.0676 |
| 10 | 4 | 2 | 5.7036 | 1.3733 | 0.1867 | 0.0860 |
| 10 | 5 | 1 | 2.8213 | 0.9125 | 0.3428 | 0.0772 |
| 10 | 5 | 2 | 3.4006 | 1.0486 | 0.4156 | 0.0517 |
| 10 | 7 | 1 | 7.3456 | 3.1376 | 0.8776 | 0.2061 |
| 10 | 7 | 2 | 4.2626 | 1.0628 | 0.1663 | 0.1314 |
| 10 | 15 | 1 | 19.2991 | 14.2480 | 1.0759 | 0.0340 |
| 10 | 15 | 2 | 7.0114 | 2.7615 | 0.1849 | 0.0292 |
| 13 | 3 | 1 | 14.8994 | 3.5681 | 0.0199 | 0.5633 |
| 13 | 4 | 1 | 8.5564 | 3.0085 | 0.2116 | 0.3352 |
| 13 | 5 | 1 | 7.1981 | 2.1647 | 0.3036 | 0.4254 |
| 13 | 7 | 1 | 15.9621 | 3.7382 | 0.6532 | 0.3253 |
| 13 | 15 | 1 | 20.1410 | 10.1032 | 0.4304 | 1.6315 |
| 15 | 3 | 1 | 13.0526 | 2.9882 | 0.0838 | 0.0715 |
| 15 | 4 | 1 | 26.8834 | 8.1055 | 0.1196 | 0.1948 |
| 15 | 4 | 2 | 0.3157 | 0.0169 | 0.1039 | 0.1379 |
| 15 | 5 | 1 | 44.5687 | 9.7412 | 0.3016 | 0.0786 |
| 15 | 5 | 2 | 0.6237 | 0.0247 | 0.0098 | 0.2388 |
| 16 | 3 | 1 | 5.1983 | 0.7456 | 0.0195 | 0.2619 |
| 16 | 4 | 1 | 7.6114 | 1.5173 | 0.0510 | 0.1431 |
| 16 | 4 | 2 | 1.2226 | 0.2419 | 0.0190 | 0.1142 |
| 16 | 5 | 1 | 17.0381 | 3.3806 | 0.1261 | 0.0570 |
| 16 | 5 | 2 | 7.4397 | 1.8530 | 0.1101 | 0.1405 |
| 18 | 3 | 1 | 1.4077 | 0.0000 | 0.0000 | 0.2586 |
| 18 | 7 | 1 | 0.1885 | 0.0000 | 0.0000 | 0.9535 |
| 20 | 3 | 1 | 0.4058 | 0.0257 | 0.0076 | 0.2140 |
| 20 | 4 | 1 | 7.4714 | 3.0853 | 0.0115 | 0.1478 |
| 20 | 4 | 2 | 7.8030 | 1.2875 | 0.0505 | 0.1149 |
| 20 | 5 | 1 | 2.0994 | 0.3146 | 0.0000 | 0.2934 |
| 20 | 5 | 2 | 3.3579 | 0.7320 | 0.0811 | 0.1607 |
| 20 | 7 | 1 | 0.5222 | 0.0378 | 0.0000 | 0.4082 |
| 20 | 7 | 2 | 13.6571 | 4.4611 | 0.2402 | 0.1100 |
| 20 | 15 | 1 | 0.4687 | 0.0391 | 0.0033 | 0.8360 |
| 20 | 15 | 2 | 16.9158 | 11.1431 | 0.4222 | 0.2930 |
| 21 | 4 | 1 | 20.1451 | 5.9981 | 0.3831 | 0.1274 |
| 21 | 7 | 1 | 14.4498 | 5.2617 | 1.7381 | 0.1088 |
| 22 | 3 | 1 | 24.7057 | 4.4770 | 0.0352 | 0.1818 |
| 22 | 4 | 1 | 20.6325 | 5.4021 | 0.1707 | 0.1613 |
| 22 | 5 | 1 | 19.6620 | 4.9759 | 0.3147 | 0.2005 |
| 22 | 7 | 1 | 25.8583 | 7.3746 | 0.7954 | 0.3576 |
| 22 | 15 | 1 | 22.0049 | 9.7484 | 0.8297 | 0.2798 |
| 28 | 3 | 1 | 6.3630 | 1.1301 | 0.0372 | 0.1303 |
| 28 | 4 | 1 | 6.2272 | 1.1718 | 0.1281 | 0.2226 |
| 28 | 15 | 1 | 12.7274 | 7.2239 | 1.1391 | 0.6584 |
| 43 | 3 | 1 | 29.0401 | 4.5319 | 0.0505 | 0.5172 |
| 43 | 4 | 1 | 29.3971 | 9.5485 | 0.6432 | 0.3236 |
| 43 | 5 | 1 | 26.0545 | 6.3729 | 0.5631 | 0.9658 |
| 43 | 7 | 1 | 29.4153 | 15.3730 | 2.4781 | 0.0902 |
| 43 | 15 | 1 | 35.1837 | 15.5455 | 0.9446 | 0.0106 |

## Extended Data Table 4 | Immunoglobulin gene usage of S-binding mAbs

| | | Heavy Chain | | | | Light Chain | | | |
|---|---|---|---|---|---|---|---|---|---|
| **Name** | **Native isotype** | **Gene usage** | **Nucleotide mutations*** | **AA mutations** | **HCDR3** | **Gene usage** | **Nucleotide mutations*** | **AA mutations** | **LCDR3** |
| 07.1A11 | IgM | VH3-15 DH1-7 JH4 | 4/283=0.0141 | 4 | TTGWFTGTYGDYFDY | VK1-33 JK4 | 1/267=0.0037 | 1 | QQYDNLPPT |
| 07.1A12 | IgA1 | VH3-49 D2-15 JH4 | 3/281=0.0107 | 3 | TRVKYCSGGSCYGYHFDH | VK3-15 JK3 | 4/262=0/0.0153 | 3 | QQYNNWFT |
| 07.1E10 | IgG1 | VH4-34 D6-19 JH6 | 5/272=0.0184 | 5 | ARVVIAVAGTYPIQVYYYYGMDV | VK1-27 JK1 | 2/266=0.0075 | 2 | QKYNSAPRT |
| 07.1E11 | IgA1 | VH3-30 D3-22 JH6 | 1/278=0.0036 | 1 | AKEEMIEDWGMDV | VL3-1 JL2 | 2/265=0.0075 | 2 | QAWDRSTVV |
| 07.1H09 | IgG1 | VH3-66 DH3-10 JH3 | 3/275=0.0109 | 3 | ARDFREGAFDI | VK1-9 JK4 | 0/266=0 | 0 | QQLNSYPPT |
| 07.2A07 | IgG1 | VH3-21 DH2-21 JH4 | 6/277=0.0217 | 6 | ARAGFVPKRAYCGGDCWYYFDY | VK3-11 JK4 | 0/263=0 | 0 | QQRSNWLT |
| 07.2A08 | IgG1 | VH4-4 DH6-19 JH4 | 2/275=0.0073 | 2 | ATDGGWYTFDH | VL3-1 JL2 | 3/265=0.0113 | 3 | QAWGSSTVV |
| 07.2A10 | IgG1 | VH4-31 DH3-16 JH3 | 1/278=0.0036 | 1 | ARYPVWGAFDI | VK1-33 JK3 | 3/267=0.0112 | 3 | QHYDNLPPT |
| 07.2C08 | IgG1 | VH1-58 DH2-15 JH3 | 2/275=0.0073 | 2 | AAAYCSGGSCSDGFDI | VK3-20 JK1 | 5/266=0.0188 | 5 | QQYGSSPWT |
| 07.2C12 | IgG1 | VH3-30-3 DH1-26 JH3 | 3/277=0.0108 | 3 | ARARGGSYSGAFDI | VK3-20 JK2 | 1/267=0.0037 | 1 | QQYGSSPMYT |
| 07.3D07 | IgG1 | VH3-30-3 DH5-18 JH4 | 3/277=0.0108 | 3 | ARVLWLRGMFDY | VL6-57 JL3 | 2/278=0.0072 | 1 | QSYDISNHWV |
| 07.4A07 | IgG1 | VH3-30-3 DH3-10 JH4 | 3/277=0.0108 | 2 | ARGDYYGSGSYPGKTFDY | VK1-33 JK4 | 1/266=0.0038 | 1 | QQYDNLPLT |
| 07.4B05 | IgG1 | VH1-69 DH1-26 JH5 | 1/277=0.0036 | 1 | ARGRLDSYSGSYYSWFDP | VK4-1 JK2 | 2/283=0.0071 | 2 | QQYYSTPYT |
| 07.4C10 | IgG1 | VH3-23 DH3-22 JH4 | 1/276=0.0036 | 1 | AKNEMAMIVVVITLFDY | VL1-51 JL3 | 2/277=0.0072 | 2 | GTWDRSLSAWV |
| 07.4D09 | IgG1 | VH4-4 DH2-15 JH4 | 1/274=0.0036 | 1 | ATKYCSGGSCSYFGY | VL2-23 JL3 | 0/277=0 | 0 | CSYAGSSTWV |
| 20.1A12 | IgG1 | VH3-30 DH1-26 JH4 | 2/277=0.0072 | 2 | AKGHSGSYRAPFDY | VK3-20 JK2 | 0/263=0 | 0 | QQYGSSYT |
| 20.2A03 | IgM | VH3-33 DH3-10 JH4 | 1/278=0.0036 | 1 | AREAYFGSGSSPDY | VL3-10 JL2 | 2/272=0.0074 | 2 | YSTDSSDNHRRV |
| 20.3C08 | IgG1 | VH3-7 DH3-22 JH4 | 1/278=0.0036 | 1 | AREGTYYYDSSAYYNGGLDY | VL3-10 JL2 | 2/268=0.0075 | 2 | YSTDSGGNPQGV |
| 20.3D12 | IgG1 | VH3-33 DH1-1 JH4 | 7/278=0.0252 | 7 | ATEPVQLEPEVRLDY | VL3-10 JL1 | 1/272=0.0037 | 1 | YSTDSSGNHRRL |
| 20.3F12 | IgG1 | VH3-7 DH4-11 JH4 | 0/278=0 | 0 | ARDQGVTTGPFDY | VL3-1 JL2 | 1/265=0.0038 | 1 | QAWDSSTVV |
| 22.1A11 | IgG3 | VH3-30-3 DH3-16 JH4 | 0/278=0 | 0 | ARDLVVWEELAGGY | VL3-10 JL3 | 2/270=0.0074 | 2 | YSTDSSGNHGV |
| 22.1B04 | IgG1 | VH3-30 DH2-15 JH4 | 4/279=0.0143 | 3 | AKQGGGTYCGGGSCYRGYFDY | VK1-33 JK4 | 2/266=0.0075 | 2 | QQYDNLPLT |
| 22.1B08 | IgA1 | VH1-46 DH4-17 JH3 | 16/278=0.0576 | 15 | ARDPRVPAVTNVNDAFDL | VK3-11 JK2 | 5/267=0.0187 | 5 | QQRSNRPPRWT |
| 22.1B12 | IgG1 | VH3-53 DH3-10 JH4 | 8/273=0.0293 | 5 | ARSHLEVRGVFDN | VK4-1 JK2 | 1/282=0.0035 | 1 | QQYYSTPCS |
| 22.1C02 | IgG1 | VH3-20 DH7-27 JH4 | 5/275=0.0182 | 4 | ARGTGAADY | VK3-20 JK2 | 6/266=0.0226 | 6 | QQYGRSPYT |
| 22.1E07 | IgA1 | VH3-33 DH4-17 JH4 | 3/278=0.0108 | 3 | AREGVYGDIGGAGLDY | VL3-10 JL1 | 4/272=0.0147 | 2 | YSTDSSVNGRV |
| 22.1E11 | IgG1 | VH3-30 DH2-15 JH4 | 2/274=0.0073 | 2 | AKMGGVYCSAGNCYSGRLEY | VK1-33 JK3 | 0/263=0 | 0 | QQYDNLLT |
| 22.1G10 | IgG1 | VH4-59 DH2-21 JH5 | 12/275=0.0436 | 11 | ARETVNNWVDP | VK4-1 JK1 | 10/282=0.0355 | 8 | QQYFTTPWT |
| 22.2A06 | IgG3 | VH5-51 DH3-3 JH4 | 1/277=0.0036 | 1 | ARREWGGSLGHIDY | VL6-57 JL2 | 4/276=0.0145 | 4 | QSFDSSNVV |
| 22.2A08 | IgG1 | VH4-59 DH2-2 JH6 | 4/274=0.0146 | 4 | ARGQGVPAALYGMDV | VL1-40 JL2 | 3/281=0.0107 | 3 | QSYDGSLSGSV |
| 22.2B06 | IgM | VH3-53 DH1-1 JH6 | 2/275=0.0073 | 2 | ARDLQLYGMDV | VL3-21 JL2 | 2/268=0.0075 | 2 | QVWDSSSDPVV |
| 22.2F03 | IgM | VH1-18 DH6-13 JH6 | 1/277=0.0036 | 1 | ARVPGLVGYSSSWYDNEKNYYYYYGMDV | VL3-25 JL1 | 1/270=0.0037 | 1 | QSADSSGTYV |
| 22.3A06 | IgG1 | VH3-23 DH5-18 JH5 | 2/277=0.0072 | 2 | AKADTAMAWYNWFDP | VK3-11 JK4 | 3/264=0.0114 | 3 | QHRSNWPLT |
| 22.3A11 | IgG1 | VH4-34 DH7-27 JH2 | 1/270=0.0037 | 1 | ARVWVRWWYFDL | VL3-21 JL1 | 4/272=0.0147 | 4 | QVWDNSSDQPNYV |
| 22.3A12 | IgG1 | VH1-46 DH2-21 JH4 | 4/275=0.0145 | 4 | ASSLPARGGVPGRLNY | VL1-51 JL2 | 3/277=0.0108 | 3 | GTWDSSLSVVV |
| 22.3D11 | IgG1 | VH5-51 D4-17 JH5 | 1/278=0.0036 | 1 | ARHHLDYDDYVGHWFDP | VL1-40 JL3 | 0/281=0 | 0 | QSYDSSLSGSGV |
| 22.3F08 | IgG1 | VH1-18 DH2-2 JH6 | 4/275=0.0145 | 4 | ASCPRRPAAIGDYYGMDV | VL3-21 JL7 | 1/271=0.0037 | 1 | QVWDSSSYHAV |

*V-region nonsynonymous nucleotide substitutions

**Extended Data Table 5 | Template switch sequences, constant region primers, and isotype-specific internal constant region sequences for bulk BCR sequencing and processing**

| **Template switch sequences** | |
|---|---|
| TS-shift0 | TACGGG |
| TS-shift1 | ATACGGG |
| TS-shift2 | TCTACGGG |
| TS-shift3 | CGATACGGG |
| TS-shift4 | GATCTACGGG |

| **Constant region primers** | |
|---|---|
| Human-IGHM | GAATTCTCACAGGAGACGAGG |
| Human-IGHD | TGTCTGCACCCTGATATGATGG |
| Human-IGHA | GGGTGCTGYMGAGGCTCAG |
| Human-IGHE | TTGCAGCAGCGGGTCAAGG |
| Human-IGHG | CCAGGGGGAAGACSGATG |
| Human-IGK | GACAGATGGTGCAGCCACAG |
| Human-IGL | AGGGYGGGAACAGAGTGAC |

| **Isotype-specific internal constant region sequences** | |
|---|---|
| Human-IGHA-InternalC | GGCTGGTCGGGGATGC |
| Human-IGHD-InternalC | GAGCCTTGGTGGGTGC |
| Human-IGHE-InternalC | GGCTCTGTGTGGAGGC |
| Human-IGHG-InternalC | GGCCCTTGGTGGARGC |
| Human-IGHM-InternalC | GGGCGGATGCACTCCC |
| Human-IGKC-IGKJ-InternalC | TTCGTTTRATHTCCAS |
| Human-IGLC-1-InternalC | TGGGGTTGGCCTTGGG |
| Human-IGLC-2-InternalC | AGGGGGCAGCCTTGGG |
| Human-IGLC-3-InternalC | YRGCCTTGGGCTGACC |
| Human-IGLC-4-InternalC | GCTGCCAAACATGTGC |

## Extended Data Table 6 | Processing of bulk sequencing BCR reads

| Participant | Sample | Cell Count | Sequence Count | | | |
|---|---|---|---|---|---|---|
| | | | Input | Preprocessed | Post-QC Productive Heavy Chains | Unique Heavy Chain VDJs |
| 07 | d28 blood plasmablast | 8361 | 2307288 | 8294 | 6031 | 3014 |
| 20 | d28 blood plasmablast | 6136 | 2068139 | 2320 | 1453 | 951 |
| 22 | d28 blood plasmablast | 15496 | 1801330 | 16126 | 13733 | 6266 |
| 07 | d28 lymph node germinal centre | 25754 | 1104539 | 2429 | 1700 | 1211 |
| 22 | d28 lymph node germinal centre | 10236 | 2117620 | 552 | 364 | 268 |

nature research

Corresponding author(s): Ali H. Ellebedy

Last updated by author(s): Jun 12, 2021

# Reporting Summary

Nature Research wishes to improve the reproducibility of the work that we publish. This form provides structure for consistency and transparency in reporting. For further information on Nature Research policies, see Authors & Referees and the Editorial Policy Checklist.

## Statistics

For all statistical analyses, confirm that the following items are present in the figure legend, table legend, main text, or Methods section.

| n/a | Confirmed | |
|---|---|---|
| ☐ | ☒ | The exact sample size (*n*) for each experimental group/condition, given as a discrete number and unit of measurement |
| ☐ | ☒ | A statement on whether measurements were taken from distinct samples or whether the same sample was measured repeatedly |
| ☐ | ☒ | The statistical test(s) used AND whether they are one- or two-sided<br>*Only common tests should be described solely by name; describe more complex techniques in the Methods section.* |
| ☒ | ☐ | A description of all covariates tested |
| ☒ | ☐ | A description of any assumptions or corrections, such as tests of normality and adjustment for multiple comparisons |
| ☐ | ☒ | A full description of the statistical parameters including central tendency (e.g. means) or other basic estimates (e.g. regression coefficient) AND variation (e.g. standard deviation) or associated estimates of uncertainty (e.g. confidence intervals) |
| ☐ | ☒ | For null hypothesis testing, the test statistic (e.g. *F*, *t*, *r*) with confidence intervals, effect sizes, degrees of freedom and *P* value noted<br>*Give P values as exact values whenever suitable.* |
| ☒ | ☐ | For Bayesian analysis, information on the choice of priors and Markov chain Monte Carlo settings |
| ☒ | ☐ | For hierarchical and complex designs, identification of the appropriate level for tests and full reporting of outcomes |
| ☒ | ☐ | Estimates of effect sizes (e.g. Cohen's *d*, Pearson's *r*), indicating how they were calculated |

*Our web collection on statistics for biologists contains articles on many of the points above.*

## Software and code

Policy information about availability of computer code

| | |
|---|---|
| Data collection | Flow cytometry data were acquired using SpectroFlo software v2.2. |
| Data analysis | Flow cytometry data were analyzed using FlowJo v10 and Prism v8. ELISA, ELISpot, and neutralization data were analyzed using Prism v8. Sequence data were analyzed using blastn v2.11.0, pRESTO v0.6.2, cd-hit-est v4.8.1, IgBLAST v1.17.1, IMGT/GENE-DB release 202113-2, Change-O v1.0.2, TIgGER v1.0.0, igraph v1.2.5, and SHazaM v1.0.2. |

For manuscripts utilizing custom algorithms or software that are central to the research but not yet described in published literature, software must be made available to editors/reviewers. We strongly encourage code deposition in a community repository (e.g. GitHub). See the Nature Research guidelines for submitting code & software for further information.

## Data

Policy information about availability of data

All manuscripts must include a data availability statement. This statement should provide the following information, where applicable:

- Accession codes, unique identifiers, or web links for publicly available datasets
- A list of figures that have associated raw data
- A description of any restrictions on data availability

Antibody sequences are deposited on GenBank under the following accession numbers: MW926396–MW926407, MW926409–MW926430, MW926432–MW926441, MZ292481–MZ292510, available from GenBank/EMBL/DDBJ. Bulk sequencing reads are deposited on Sequence Read Archive under BioProject PRJNA731610. The IMGT/V-QUEST database is accessible at http://www.imgt.org/IMGT_vquest/. Other relevant data are available from the corresponding author upon request.

# Field-specific reporting

Please select the one below that is the best fit for your research. If you are not sure, read the appropriate sections before making your selection.

☒ Life sciences ☐ Behavioural & social sciences ☐ Ecological, evolutionary & environmental sciences

For a reference copy of the document with all sections, see nature.com/documents/nr-reporting-summary-flat.pdf

# Life sciences study design

All studies must disclose on these points even when the disclosure is negative.

| | |
|---|---|
| Sample size | No statistical methods were used to determine sample size. 41 total participants were enrolled based on recruitment, of whom 14 provided axillary LN samples |
| Data exclusions | No data were excluded |
| Replication | Human samples were collected from 41 participants. For ELISA, ELISpot, and neutralization assays, results were from one experiment performed in duplicate. Flow cytometry experiments were performed once |
| Randomization | Different experimental groups were not used. |
| Blinding | No blinding was done for convenience; subjective measurements were not made. |

# Reporting for specific materials, systems and methods

We require information from authors about some types of materials, experimental systems and methods used in many studies. Here, indicate whether each material, system or method listed is relevant to your study. If you are not sure if a list item applies to your research, read the appropriate section before selecting a response.

## Materials & experimental systems

| n/a | Involved in the study |
|---|---|
| ☐ | ☒ Antibodies |
| ☐ | ☒ Eukaryotic cell lines |
| ☒ | ☐ Palaeontology |
| ☒ | ☐ Animals and other organisms |
| ☐ | ☒ Human research participants |
| ☒ | ☐ Clinical data |

## Methods

| n/a | Involved in the study |
|---|---|
| ☒ | ☐ ChIP-seq |
| ☐ | ☒ Flow cytometry |
| ☒ | ☐ MRI-based neuroimaging |

## Antibodies

| | |
|---|---|
| Antibodies used | total Ig (goat polyclonal, Jackson ImmunoResearch 109-005-064), IgG-HRP (goat polyclonal, Jackson ImmuoResearch 109-035-088), IgA-HRP (goat polyclonal, Jackson ImmuoResearch 109-035-011), IgM-HRP (goat polyclonal, Caltag H15007), mouse IgG-HRP (goat polyclonal, Sigma 12-349), murine anti-S mAbs: SARS2-2, SARS2-11, SARS2-16, SARS2-31, SARS2-38, SARS2-57, and SARS2-71 (Diamond laboratory, Washington University School of Medicine), IgG-BV480 (goat polyclonal, Jackson Immunoresearch 109-685-098), PD-1-BB515 (EH12.1, BD Horizon 564494), IgA-FITC (M24A, Millipore CBL114F), CD45-A532 (HI30, Thermo 58-0459-42), Bcl6-PE (K112-91, 561522, BD Pharmingen), CD38-BB700 (HIT2, 566445, BD Horizon), Blimp1-A700 (646702, IC36081N, R&D), CD19-BV421 (HIB19, 302234), FoxP3-BV421 (206D, 320124), CD20-Pacific Blue (2H7, 302320), CD27-BV510 (O323, 302836), CD8-BV570 (RPA-T8, 301038), IgM-BV-605 (MHM-88, 314524), HLA-DR-BV650 (L243, 307650), Ki-67-BV711 (Ki-67, 350516), CD19-BV750 (HIB19, 302262), Tbet-BV785 (4B10, 644835), CD3-FITC (HIT3a, 300306), CD71-FITC (CY1G4, 334104), IgD-PE (IA6-2, 348204), CD71-PE (CY1G4, 334106), CXCR5-PE-Dazzle 594 (J252D4, 356928), IgD-PE-Cy5 (IA6-2, 348250), CD4-PerCP (OKT4, 317432), CD14-PerCP (HCD14, 325632), IgD-PerCP-Cy5.5 (IA6-2, 348208), CD38-PE-Cy7 (HIT2, 303516), CD71-PE-Cy7 (CY1G4, 334112), CD19-APC (HIB19, 302212), CD4-Spark 685 (SK3, 344658), CD20-APC-Fire750 (2H7, 302358), CD3-APC-Fire810 (SK7, 344858); all Biolegend. |
| Validation | All commercial antibodies were validated by their manufacturers as detailed in their product information and titrated in the lab for the indicated assay by serial dilution. We validated mAbs generated in our lab in preliminary ELISAs to SARS-CoV-2 spike, bovine serum albumin, and anti-Ig. |

## Eukaryotic cell lines

Policy information about cell lines

| | |
|---|---|
| Cell line source(s) | Expi293F (Thermo), Vero E6 (CRL-1586, American Type Culture Collection), Vero-TMPRSS2 (Ding laboratory, Washington University School of Medicine), Vero-hACE2-TMPRSS2 (Graham laboratory, VRC/NIH) |
| Authentication | All cell lines grew and performed as expected. Expression of TMPRSS2 on Vero-TMPRSS2 was validated by flow cytometry [ref. 17]. No additional specific authentication was performed. |
| Mycoplasma contamination | Vero lines were tested monthly for mycoplasma and were negative. Expi293F lines were not tested. |
| Commonly misidentified lines (See ICLAC register) | No commonly misidentified cell lines were used |

## Human research participants

Policy information about studies involving human research participants

| | |
|---|---|
| Population characteristics | Study participants demographics are detailed in Extended Data Table 1 |
| Recruitment | Study participants were recruited from the St. Louis metropolitan area by the Washington University Clinical Trials Unit. Potential self-selection and recruiting biases are unlikely to affect the parameters we measured. |
| Ethics oversight | The study was approved by the Washington University IRB |

Note that full information on the approval of the study protocol must also be provided in the manuscript.

## Flow Cytometry

### Plots

Confirm that:

☒ The axis labels state the marker and fluorochrome used (e.g. CD4-FITC).

☒ The axis scales are clearly visible. Include numbers along axes only for bottom left plot of group (a 'group' is an analysis of identical markers).

☒ All plots are contour plots with outliers or pseudocolor plots.

☒ A numerical value for number of cells or percentage (with statistics) is provided.

### Methodology

| | |
|---|---|
| Sample preparation | Fine needle aspirates of axillary LNs were flushed from needles with 3 mL of RPMI supplemented with 10% FBS and 100 U/mL penicillin/streptomycin, followed by three 1 mL rinses. Red blood cells were lysed with ammonium chloride buffer, washed twice with PBS supplemented with 2% FBS, 2mM EDTA and immediately used or cryopreserved in 10% DMSO in FBS.<br>Blood samples were collected in EDTA tubes, and peripheral blood mononuclear cells (PBMCs) were enriched by density gradient centrifugation over Ficoll 1077 (GE) or Lymphopure (BioLegend). The residual red blood cells were lysed with ammonium chloride lysis buffer, and cells were immediately used or cryopreserved in 10% dimethylsulfoxide in FBS. |
| Instrument | Cytek Aurora |
| Software | Flow cytometry data was acquired using Cytek SpectroFlo and analyzed using FlowJo (Treestar) v10. |
| Cell population abundance | Single cell sorts and bulk sorts directly into lysis buffer were not amenable to post-sort purity analysis. |
| Gating strategy | Gating strategies are shown in Extended Data Figure 2 |

☒ Tick this box to confirm that a figure exemplifying the gating strategy is provided in the Supplementary Information.